

Orbital stability of compact three-planet systems

III. The role of three-body resonances

S. Gavino¹ and J. J. Lissauer²

¹ Dipartimento di Fisica e Astronomia, Università di Bologna, Via Gobetti 93/2, 40122, Bologna, Italy; Niels Bohr Institute and Centre for Star and Planet Formation, University of Copenhagen, Øster Voldgade 5-7, 1350, Copenhagen K, Denmark

² Space Science & Astrobiology Division, MS 245-3, NASA Ames Research Center, Moffett Field, CA 94035, USA

Received 2025; accepted 2026

ABSTRACT

Context. Observational surveys show that at least $\sim 30\%$ of short-period multiplanet systems host tightly packed planets, some of which are locked in stable chains of mean-motion resonances. Despite recent progress, the dynamical stability of these systems remains only partially understood. Numerical simulations have established a general exponential increase in system lifetime with orbital separation, with mean-motion resonances playing a key role in regulating stability. Tightly packed three-planet systems exhibit a distinctive behavior not seen in higher-multiplicity systems: a small yet significant region of phase space is anomalously stable.

Aims. This study investigates the dynamics of extremely compact three-planet systems, focusing on anomalously long-lived configurations and their connection to resonant chains observed in exoplanetary systems.

Methods. We perform numerical integrations of coplanar, initially circular, equal-mass three-planet systems over stellar-lifetime timescales and at high resolution in orbital separation, and interpret the results in the context of recent analytical work.

Results. We identify regions of phase space hosting anomalously stable orbits, including systems surviving multiple orders of magnitude longer than predicted by the exponential trend.

Conclusions. We demonstrate a clear link between stability and isolated three-body mean-motion resonances, showing that extremely compact systems can remain stable when captured into a small subset of isolated zeroth-order resonances. Stability further depends on the initial orbital longitudes and on the interplay between the three-body and two-body resonance networks.

Key words. Stars: exoplanets – numerical – planetary systems – planets and satellites – dynamical evolution and stability

1. Introduction

Approximately 1000 multiplanet systems have been identified in recent decades, most by NASA's *Kepler* (Lissauer et al. 2011a,b; Fabrycky et al. 2014; Lissauer et al. 2024) and *TESS* space telescopes. Hundreds of these systems contain three or more super-Earth and/or sub-Neptune planets on nearly co-planar orbits in compact systems, and many individual systems show an approximate uniformity in mass and orbital spacing (Millholland et al. 2017; Weiss et al. 2018, 2023). The formation route to such system's architectures has been discussed recently (e.g., Goldberg & Batygin 2022; Tejada Arevalo et al. 2022), but many questions remain unanswered. In particular, although simulations suggest that planets are typically captured in mean motion resonance (MMR) chains due to planet-disk interactions, studies show that planetary systems can become unstable once the dissipative action of the disk stops and observations indicate that the majority of tightly-packed systems possess orbits away from resonant configurations (e.g., Fabrycky et al. 2014; Batygin & Adams 2017; Izidoro et al. 2017; Pichierri & Morbidelli 2020; Izidoro et al. 2021). Indeed, the probability of a multiplanet system being locked in a resonant chain is observed to decrease with system age (Dai et al. 2024). Nevertheless, even though the fraction of observed resonant chains among old planetary systems is small,

understanding the conditions that ensure their stability may help elucidate why these resonant configurations are uncommon.

Analytical studies of two-planet systems have provided a satisfactory characterization of their dynamical stability (Hill 1878). Stability criteria are mostly based on orbital spacing (e.g., Gladman 1993) or based on the overlap of mean motion resonances (e.g., Chirikov 1979; Wisdom 1980; Deck et al. 2013; Hadden & Lithwick 2018).

However, deriving analytical stability criteria becomes significantly more challenging for systems containing three or more planets. Many authors have used numerical integrations to determine the mechanisms that lead to instability in these systems. In most cases, these studies are restricted to the idealized case of systems of equal-mass planets on equally-spaced (in terms of period ratios of neighboring planets) orbits. Although these intensively-studied systems are 'idealized', they have been an effective tool to derive general dynamical trends in planetary systems. The first numerical investigation was done by Chambers et al. (1996). Successive studies focused on specific numbers of planets (e.g., Obertas et al. 2017; Lissauer & Gavino 2021; Outland et al. 2026), different masses (e.g., Smith & Lissauer 2009; Morrison & Kratter 2016; Rice & Steffen 2023), initial orbital eccentricities (Gratia & Lissauer 2021) or systems with co-orbital planets (Smith & Lissauer 2010). All of these works have shown the general trend that the system's lifetime increases exponentially with increasing initial orbital spacing.

Send offprint requests to: Sacha Gavino
e-mail: sacha.gavino@unibo.it

Other authors have derived analytical or semi-analytical solutions to predict survival time of systems with more than two planets. In particular, Quillen (2011) introduced a resonance overlap criterion to estimate the role of three-body mean motion resonances (3BRs) causing destabilization in tightly-packed multiplanet systems. More recently, Petit et al. (2020) (henceforth PPDJ20) presented an analytical model that estimates compact systems' lifetimes based on the overlap of zeroth-order 3BRs. Subsequently, Petit (2021) developed an integrable model for first-order 3BRs by generalizing a similar approach to that used for two-planet systems.

Systems with three planets represent about a quarter of all multiplanetary systems in the *Kepler* planet candidate catalog (Lissauer et al. 2024), and constitute a bridge between the dynamically well-characterized one- and two-planet systems, and general multi-planet systems. Numerical simulations of three-planet systems (Lissauer & Gavino 2021; henceforth Paper I) have shown specific behavior that was not reported in numerical simulations with more planets (Smith & Lissauer 2009; Obertas et al. (2017) hereafter OVT17; Outland et al. (2026)).

This present work is an extension of Paper I and (Bartram et al. 2021; henceforth Paper II) who attempted an effort to fill the gap by quantitatively characterizing the lifetime dependence to the orbital spacing of circular tightly-packed three-planet systems and explored the post-instability impact behavior as a function of the (physical, not orbital) radii of the planets. As for systems with four or more planets, they found that three-planet systems follow a trend where the system's lifetime increases approximately exponentially with the initial orbital separation, although three-planet systems tend to be globally longer-lived, with the magnitude of the difference increasing at larger separations. More surprisingly, they found that a notable fraction of very tightly-packed three-planet systems exhibits a peculiar behavior, due to specific pairings of orbital separation and initial longitudes, resulting in anomalous lifetimes that are multiple orders of magnitudes longer than the exponential trend. Although such systems likely constitute only a tiny fraction of all planetary systems in the galaxy, a detailed investigation is warranted, as their stability mechanisms may share features with observed tightly-packed resonant-chains that remained stable after the dissipation of the protoplanetary disk gas. This work extends the numerical investigation of anomalously stable three-planet systems initiated by Paper I, revealing links to 3BRs.

2. Numerical methods

2.1. Integration packages and duration

All integrations presented in Sects. 3 and 4 were performed using the Wisdom-Holman method MVS (mixed-variable symplectic) embedded in the Mercury software package (Chambers 1999) with a timestep of 18 days. We consider a system to be unstable when two orbits cross (more precisely, when the apoapsis of the innermost orbit becomes larger than the periapsis of the middle orbit or the apoapsis of the middle orbit becomes larger than the periapsis of the outermost orbit). Each system was integrated until it became unstable or 10^{10} initial orbital periods of the innermost planet elapsed. We call the time that elapses until the system becomes unstable or reaches the maximum integration time the lifetime of the system, although more precisely, for systems that are timed out, we only know that the lower bound on its lifetime is 10^{10} periods. The system's lifetime is denoted t_c/t_0 , where t_0 is the period of the innermost planet (1 year).

In Sects. 6, and 7, we used the WHFast integrator (Rein & Tamayo 2015; Wisdom & Holman 1991) of the N-body code REBOUND (Rein & Liu 2012) to perform further analyzes of a selection of systems of interest with the same timestep of 18 days.

2.2. Initial orbital configurations

In this study, all systems have three planets of equal mass, with each planet's mass equal to that of the Earth ($M_j = 1 M_{\oplus}$ for $j = 1, 2, 3$), orbiting a one solar mass star $M_{\star} = 1 M_{\odot}$. The systems are coplanar, and the orbits of the planets are in the same direction and initially circular. The innermost planet orbits at 1 AU from the star.

Although the Hill radius is not the most adapted measure of orbital separation, (the stability is better described by a spacing scaled as a planet-to-star mass ratio to the power of 1/4, PPDJ20), we use it nonetheless for consistency and direct comparison with similar previous studies. The mutual Hill radius of neighboring planets is defined as:

$$R_{H_{j,j+1}} \equiv X(a_j + a_{j+1}), \quad (1)$$

where a_j and a_{j+1} are the semi-major axis of the j th and $(j+1)$ th planets, respectively, and where X is

$$X \equiv \frac{1}{2} \left[\frac{2M_{\oplus}}{3(M_{\odot} + (j-1)M_{\oplus})} \right]^{\frac{1}{3}}. \quad (2)$$

The relationship between the semi-major axes of successive pairs of planets can be expressed in terms of mutual Hill radius as follows:

$$a_{j+1} = a_j + \beta R_{H_{j,j+1}}, \quad (3)$$

where we refer to β as the dynamical separation. Note that equal values of β do not imply equal orbital distances, even for equal-mass planets. A system of two planets that are initially on circular and coplanar orbits is stable if β exceeds $\approx 2\sqrt{3}$ (Gladman 1993). We say that this system is Hill stable. In the case of Earth-mass planets, this corresponds to an orbital period ratio of ~ 1.0680 .

Similarly to Obertas et al. (2017), we can use Eq. 2 to express the semi-major axes of successive pairs of planets of equal mass as follows:

$$a_{j+1} = a_j \left(\frac{1 + \beta X}{1 - \beta X} \right), \quad (4)$$

This, using Kepler's third law, allows us to express the period ratios of successive pairs as a function of orbital separation as

$$\frac{P_{j+1}}{P_j} = \left(\frac{1 + \beta X}{1 - \beta X} \right)^{\frac{3}{2}}. \quad (5)$$

We consider four sets of initial angular orbital elements, choosing coordinates such that the innermost planet begins at 0 longitude, so that the sets differ only by the middle and outer planets' longitudes. These sets of longitudes are summarized in Table 1. In the first set of runs the initial longitudes of the

middle and outer planets, λ_2 and λ_3 are randomly and independently drawn from a uniform distribution; we call this set as Random. This method is similar to, for example, those used by [Obertas et al. \(2017\)](#) and in Section 3 of [Paper I](#). Lifetimes of these systems are presented in Section 3.1. The second, third and fourth sets, Restricted Random (RR), Specific 1 (S1) and Specific 2 (S2), respectively, have the initial longitudes of the middle and outer planets with restricted values. The reason behind the choices of restricted longitudes will be given in the following sections.

3. Results: Systems with Random Initial Longitudes

3.1. Lifetime vs. orbital separation

In this section, we extend the work done by [Paper I](#) to better characterize the anomalously long-lived systems and their dependence on the initial longitudes. In order to detect anomalous systems that were not seen previously, we performed a blind search by integrating systems in the Random set with a resolution of 5×10^6 per unit β (more than three orders of magnitude finer than in [Paper I](#)) over the range $[2\sqrt{3}, 5.00]$, and a resolution of 2×10^4 within the range $(5.00, 5.60)$. The entire Random set comprises a total of more than 7,500,000 integrated systems.

Figure 1a shows the lifetime as a function of the initial separation for all integrated systems in the Random set. As shown in other studies, the systems' lifetimes, t_c , approximately follow a linear trend with the initial separation measured in $\beta' \equiv \beta - 2\sqrt{3}$ given by $\log t_c = b'\beta' + c'$, with b' and c' being constant (e.g., [Chambers et al. 1996](#); [Smith & Lissauer 2009](#); [Obertas et al. 2017](#); [Quarles & Lissauer 2018](#)) and [Paper I](#). We fit our data covering the range $(2\sqrt{3}, 5.6]$ in β using a uniform subset of resolution of 2×10^4 , which produces the values of $b' = 1.25212$ and $c' = 2.20944$. We define a system to be anomalously long-lived when its lifetime is greater than 5σ above the exponential fit, which corresponds to about two orders of magnitude larger than the exponential fit lifetime at the system's orbital separation.

3.2. Anomalous systems

Spikes corresponding to anomalously long-lived systems are clearly visible in Fig. 1, with five successive spikes identifiable. We call the first three spikes, from left to right in Fig. 1a, SPK1, SPK2, and SPK3, respectively. These spikes were not detected by [Paper I](#) due to the lower resolution in β . We further increased the resolution by a factor 2 in the SPK1 region (within the range $[3.81, 3.85]$) to help better visualize the inner structures (Fig. 1b).

Two outer spikes are visible, SPK4 and SPK5, surrounding $\beta \sim 5.15$ and $\beta \sim 5.40$, respectively, which appear to be longer-lived relative to the exponential fit than the three inner spikes. More significantly, they occupy a much larger fraction of phase space, since they have more points despite 250 or 500 times coarser resolution. Four systems survived for ten billion years in SPK4 and SPK5, and have values $\beta = 5.1547, 5.15665, 5.4135$, and 5.41885 . This means that using specific initial longitudes can allow the systems to survive for more than six orders of magnitude longer than the lifetime approximated by the exponential fit. Note that these two spikes were already found by [Paper I](#).

The spikes are not uniformly spaced along the horizontal axis in Fig. 1. In particular, we can see a wide region between SPK3 and SPK4 where no spikes were found, which corresponds to a gap of approximately 0.60 in β (between $\beta \approx 4.55$ and $\beta \approx$

5.15). This suggests that the inner and outer spikes may originate from different mechanisms. The origin of this wide region will be discussed in Section 6.3.

Similarly to [Paper I](#), we find that specific combinations of initial conditions lead to anomalous long-term stability. In this work, three additional inner spikes are detected, SPK1, SPK2 and SPK3. The distribution of the spike systems as a function of the initial angles is presented in Figure 2.

For the three inner spikes seen in Fig. 1, we find 18 (34 including the higher resolution shown in Fig. 1b), 33, and 23 systems in SPK1, SPK2, SPK3, respectively. From the figure, we see a clear correlation between the initial conjunction of the outer pair of planets and the dynamical stability. In total, 34, 30, and 7 systems, in SPK1, SPK2, and SPK3, respectively, start in the immediate vicinity of the curve $\lambda_2 = \lambda_3 (\pm 2^\circ)$, which corresponds to 100%, 91% and 30% of all systems in SPK1, SPK2, and SPK3, respectively. This result should be considered with a strong caveat that will be discussed in Section 6.2.

We find 43 systems in SPK4 and 39 in SPK5 despite the much coarser resolution of our simulations for these less closely-spaced systems. There do not appear to be clear angle preferences for SPK4 and SPK5, but it is possible that the small number of systems does not allow any statistical trends to be immediately visible. We know from [Paper I](#) that there is a correlation between initial angles and the stability of the systems in SPK4 and SPK5. This will be discussed in Section 6.1. There is no evident correlation in Fig. 2 between the system's lifetime and other conjunctions (of the inner pair, or between the first and third planets).

4. Lifetimes of Restricted and Specific sets

In order to determine how close-to-conjunction initial configurations affect the "strength" and shape of the spikes, we simulate an additional set of systems, called the RR set, where the initial longitude of the middle planet, λ_2 is randomly selected and the initial longitude of the outer planet, λ_3 , is randomly drawn from a range within 2° around λ_2 . We restrict the simulations inside $\beta = 4.9$ since only SPK1, SPK2, and SPK3 show a correlation with the initial conjunction, and we use a resolution of 10^{-5} in β . The results are shown in Figure 3. The equivalents of SPK1 and SPK2 are obtained again, but thinner and longer-lived. SPK3, on the other hand, does not appear to be significantly changed. Combining SPK1 and SPK2, there are 20 systems that survived for more than 10^6 years and 4 systems that survived for more than 10^7 (2 in each spike). There is also an additional notable outlier very close to the critical β value for two-planet systems ($2\sqrt{3}$) that survived for about 8×10^4 years.

From the RR set, the longest-lived system in SPK1 is the system with $\beta = 3.81563$ with a lifetime of 2.72×10^7 years and initial angles $\lambda_2 = 166.273784^\circ$ and $\lambda_3 = 165.110014^\circ$. To further restrict the angle dependence on the lifetime in SPK1, we use the initial longitude values of this system to perform another additional set of simulations, the S1 set, where all systems start with these initial angles and with the same resolution and range in β as the RR set. The result is shown in the left panel of Figure 4. Here, SPK1 is much more prominent and longer-lived than in the other sets. A total of five systems remained stable for 10^{10} years. The spike also exhibits a complex structure (Fig. 4 right) composed of many successive sub-dips and sub-spikes. In particular, the spike is divided into two major sub-spikes, one longer-lived than the other.

As mentioned above, we observe the presence of an anomalously stable system very close to the critical β value for two

Table 1: Initial planetary longitudes.^a

Sets	Section	λ_2	λ_3
Random	3	random	random
Restricted Random (RR)	4	random	$-2^\circ \leq \lambda_2 \leq 2^\circ$
Specific #1 (S1)	4	166.273784°	165.110014°
Specific #2 (S2)	4	207.16381°	208.66160°

^a Longitude values are given to precision input.

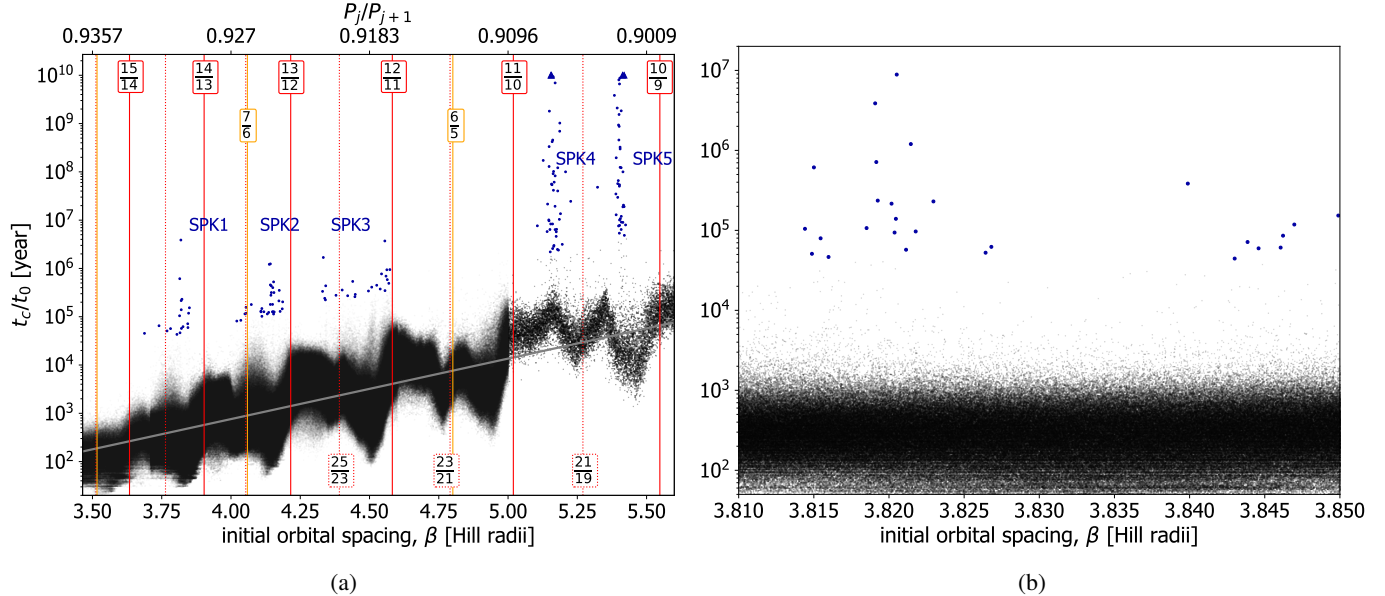


Fig. 1: Lifetime, t_c , of three-planet systems as a function of the initial separation of the orbits of neighboring planets in units of β for the set Random (initial longitudes of the middle and outer planets selected randomly). Panel (a) shows the full view with a density of 5×10^6 per unit β within the range $[2\sqrt{3}, 5.00]$, and a density of 2×10^4 within the range $(5.00, 5.60]$. Systems with a lifetime greater than 5σ above the exponential fit are shown with larger size dots that are navy blue in color. The upward-pointing triangles represent systems that remained stable for the entire elapsed time, 10^{10} years. The upper horizontal axis shows the initial period ratios of neighboring planets as defined by Eq. 5. The solid (dotted) red vertical lines denote the locations of first-order (second-order) 2BRs between adjacent pairs of planets, and the solid gold vertical lines denote first-order 2BRs between the innermost and outermost planets. The solid gray line segment represents the exponential fit to all points with a density of 10,000 per unit β within the range $[3.4645, 5.6000]$. The terms $SPKi$ denote the i th spike with $i \in [1,2,3,4,5]$. Panel (b) shows a zoomed-in view with a density of 10^7 within the range $\beta \in [3.81, 3.85]$.

planets in the RR set (Fig. 3). In order to figure out whether this system belongs to a spike or not and if a spike can exist this close to the critical value, we perform another set of simulations, the set S2, with all systems starting with the initial longitude values of this anomalous system: $\lambda_2 = 207.16381^\circ$ and $\lambda_3 = 208.66160^\circ$. From Figure 5, we confirm the presence of an extremely thin spike around $\beta = 3.4744$, which is just about 0.35% wider than the critical β value for two planets.

5. Geometry of three-body resonances

The spikes identified in Sect. 3 do not seem to be linked to any strong two-body mean motion resonances (2BRs). Another possible mechanism leading to the anomalous stability of these long-lived systems is three-body mean motion resonances (in principle, secular resonances could also be the cause). (PPDJ20) predicted that, within what they defined as the overlap limit of the three-body resonances, the dynamics of a three-planet system (that isn't close to any strong two-body mean motion reso-

nances) is driven by Chirikov diffusion (Chirikov 1979), which quickly leads the system on a chaotic path perpendicular to the resonance network. If systems within these long-lived spikes are stabilized by relatively strong three-body resonances, the presence of such systems with very small orbital period ratios (which, as we will see, are well inside the theoretical stability limit) needs to be analyzed.

This section provides the material required to address the points discussed in the following sections. The reader is referred to previous studies (e.g., Chirikov 1979; Aksnes 1988; Quillen 2011; Petit et al. 2020) for more thorough and detailed descriptions.

In the following, the mean motion of the j th planet in a system is denoted by n_j , where $j = 1, 2, 3$ and where $n_1 > n_2 > n_3$. A system is in a zeroth-order 3BR if the orbital frequencies of the three bodies are linked by the relationship:

$$\frac{p}{n_2 - n_3} = \frac{q}{n_1 - n_2} = \frac{p + q}{n_1 - n_3} \approx \frac{P_{3\text{br}}}{2\pi}. \quad (6)$$

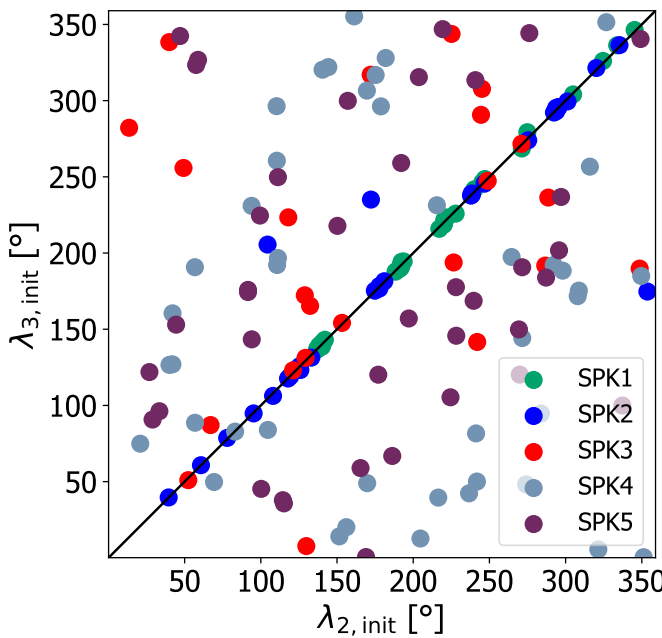


Fig. 2: Initial longitude of the middle planet versus the outer planet of systems from the Random set whose lifetimes are greater than 5σ above the exponential fit (anomalous systems), i.e., systems in SPK1, SPK2, SPK3, SPK4, and SPK5. For SPK1 we include the systems from the higher resolution batch seen on Fig. 1b. The solid black diagonal curve marks the locus of points where the outer pair of planets start in conjunction.

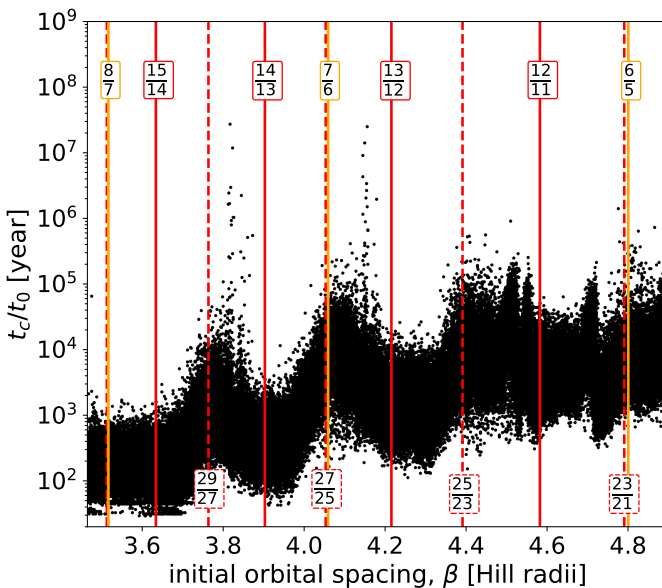


Fig. 3: Lifetime, t_c , of three-planet systems as a function of the initial separation of the orbits of neighboring planets for the RR set (see Table 1) with a fixed density of 2×10^5 per unit of β over the range $[2\sqrt{3}, 4.9000]$.

where p and q are positive integers. The recurrence period $P_{3\text{br}}$ is the interval in which the triplet of planets returns to the same initial orbital configuration (note that this periodic configuration does not necessarily occur at the same longitude in the inertial

frame). Multiplying the two leftmost equations of Eq. 6 by the denominators of both fractions and rearranging terms yields:

$$pn_1 - (p+q)n_2 + qn_3 = 0. \quad (7)$$

Integrating Eq. 7 shows that a relationship associated with the three-body resonance also exists between the three longitudes around a resonant angle ϕ :

$$p\lambda_1 - (p+q)\lambda_2 + q\lambda_3 = \phi, \quad (8)$$

where λ_1 , λ_2 , and λ_3 are the longitude of planets 1, 2, and 3, respectively. The system is in a 3BR if the resonant angle ϕ librates.

Following the same approach as in PPDJ20, we divide Eq. 7 by n_2 and isolate the new term n_3/n_2 . Noting that the ratio of mean motions is related by the ratio of the orbital periods as

$$P_j/P_{j+1} = n_{j+1}/n_j, \quad (9)$$

Eq. 7 becomes

$$\frac{P_2}{P_3} = \frac{p}{q} \left(1 - \left(\frac{P_1}{P_2} \right)^{-1} \right) + 1. \quad (10)$$

The geometry of the zeroth-order 3BRs can therefore be described in a two-dimensional plane defined by the period ratios of the inner and outer pairs (note that this is possible because zeroth-order 3BRs are independent of the longitude of the perihelion). Using Eq. 6 and Eq. 10, the ratio of the three-body resonant period $P_{3\text{br}}$ to the period of the inner planet, P_1 , can be expressed in terms of the period ratios of the outer pair only:

$$P_{3\text{br}} = qP_1 \left[1 + \frac{q}{p} \left(1 - \frac{P_2}{P_3} \right) \right] \left[\frac{q}{p} \left(1 - \frac{P_2}{P_3} \right) \right]^{-1}. \quad (11)$$

Note that the smallest possible value of $P_{3\text{br}}$ is for $q/p = 1$.

In all the following, we note $\alpha \equiv q/p$, where p and q are coprime. The indicated fraction q/p always shows the lowest terms, but it also represents all other resonances with higher terms because all resonances with the same value α lie on top of each other. We use 3BR α to denote the three-body resonances, where $\alpha = w$. Figure 6 shows the 2-D period ratio plane. The resonances 3BR $\alpha 1/2$, 3BR $\alpha 2/3$, 3BR $\alpha 1$, 3BR $\alpha 3/2$, and 3BR $\alpha 2$ are shown in bold green because they are of special importance for the discussion. Using the density of the 3BR network, which is characterized by a filling factor, PPDJ20 defined a theoretical stability limit for a triplet of planets based on the overlap of 3BRs in the period ratio plane (their Eqs. 58 and 59). The limit is represented by the blue curve in Fig. 6. Inside this curve, the overlap of zeroth-order 3BRs is such that the space is fully filled by the network. In the case of Earth-mass planets, the limit is at $P_{j+1}/P_j \approx 1.15$ for uniformly-spaced orbits. From Fig. 6, considering that the black square roughly represents the boundaries of our numerical work space, we see that the spike systems found in Sect. 3 are well within the theoretical stability limit. We call the solid black diagonal line in Fig. 6 that represents the locus of systems with the two adjacent pairs having equal period ratios, i.e., geometrically-spaced orbits, the "main diagonal". Therefore, all systems shown in Sects. 3 and 4, as well as those within Paper I and Paper II, started on the main diagonal.

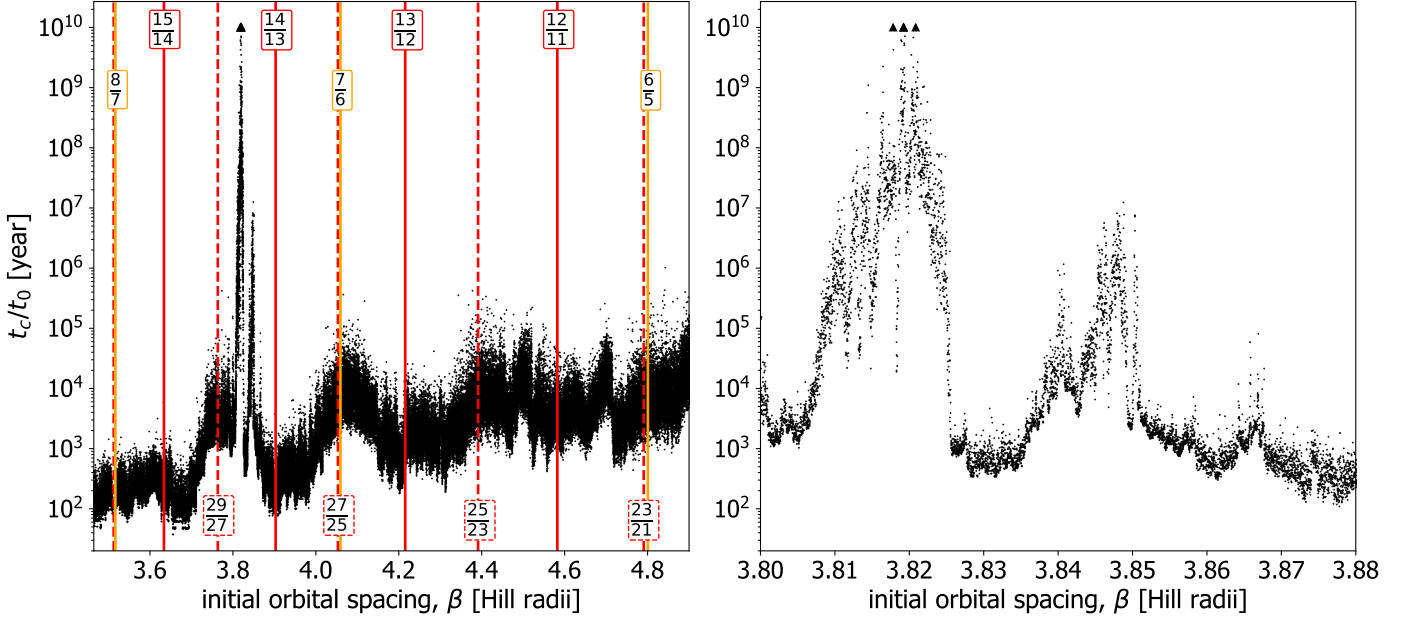


Fig. 4: Left: lifetime, t_c/t_0 , of three-planet systems as a function of the initial separation of the orbits of neighboring planets for the set S1 ($\lambda_{2,\text{init}} = 166.273784^\circ$ and $\lambda_{3,\text{init}} = 165.110014^\circ$). The triangles represent systems that remained stable for the entire time interval, 10^{10} years. There are five systems that survived for ten billion years; these systems have initial orbital separations of $\beta = 3.81783, 3.81921, 3.81922, 3.81926$, and 3.82086 . The resolution is 10^5 per unit of β . Right: zoom into the spike in the range [3.80, 3.87].

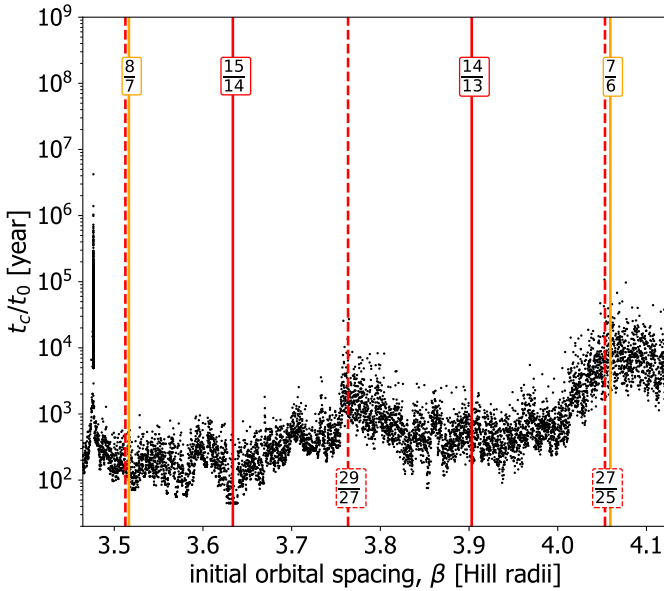


Fig. 5: Lifetime, t_c/t_0 , of three-planet systems as a function of the initial separation of the orbits of neighboring planets for the set S2 ($\lambda_{2,\text{init}} = 207.16381^\circ$ and $\lambda_{3,\text{init}} = 208.66160^\circ$). The resolution is 10^6 per unit β in the range [3.47643, 3.47645] and 10^4 elsewhere over the range [3.4645, 4.1300].

Analogously, a pair of planets is in a two-body mean motion resonance (hereafter 2BR) if the longitudes are linked by the following relationship:

$$(p' + q')\lambda_{j+1} - p'\lambda_j + q'\bar{\omega} = \phi_{2b}. \quad (12)$$

where p' and q' are also positive integers and $\bar{\omega}$ is the longitude of pericenter of the j th or $(j+1)$ th planet. The integer $q' = 1$ for first-order 2BRs, $q' = 2$ for second-order 2BRs, etc. A triplet of planets with a librating 3BR angle but without librating 2BR angles is said to be in a pure 3BR.

An important aspect is the relationship between 3BRs and 2BRs. Consider a system locked in a 3BR with p and q . If the inner pair is captured in a 2BR (of any order), we can express P_2/P_1 as a ratio $p' + q'/p'$ and Eq. 10 can be rewritten as

$$\frac{P_2}{P_3} = 1 - \frac{p' q'}{q' p'}. \quad (13)$$

We see from Eq. 13 that if a system is captured in 3BR $\alpha 1$, then the period ratio P_3/P_2 is necessarily a ratio of integers $(p'' + q'')/p''$ such that $q'' = q'$. This means that when the 3BR $\alpha 1$ crosses any k th-order 2BRs of any pair of planets, the other pair is also systematically in a k th-order 2BR at the intersection. This is specific to the 3BR $\alpha 1$, although other 3BRs also have a similar periodicity of 2BRs crossings. For example, the 3BR $\alpha 2$ alternates between intersections of 2BRs of different order and 2BRs of the same order (see Fig. 6). More generally, all resonances with a pair p and q such that the ratio p/q has the same value lie on top of each other (i.e., when p and q are not coprime). The more 3BRs lie on top of each other, the larger the density of intersection crossings of 2BRs, and the more isolated they are from the rest of the network. The 3BR $\alpha 1$ is the one that exhibits the largest density of intersection crossings in the plane and is the most isolated of the 3BR network. The 3BR $\alpha 2$ is the second most isolated, etc. These 3BRs are therefore important for the stability of triplets of planets, in particular where the 3BR network is very dense, because a system near one of these resonances is more likely to remain safe from Chirikov diffusion and is more likely to be driven by 2BRs. More about the geometry of three-body resonance is given in Appendix B.

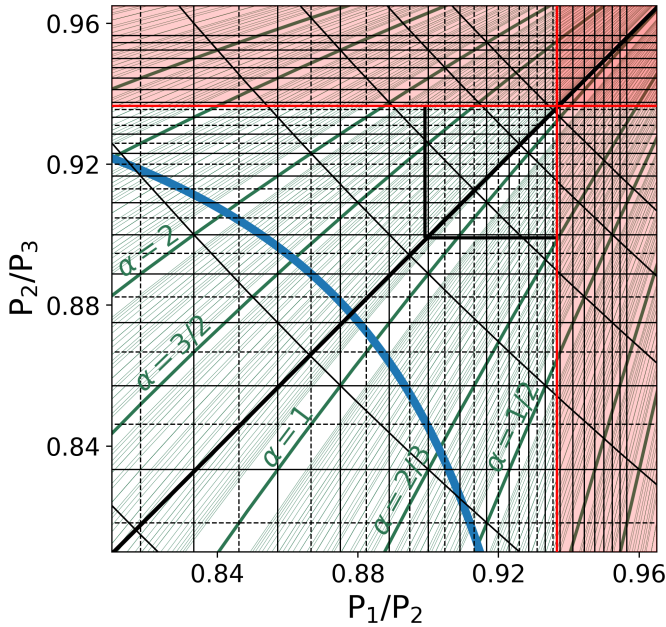


Fig. 6: Resonance locations and stability boundaries are displayed within the period ratio plane. The red lines and shaded areas are the two-planet Hill-stability limits for circular orbits (Gladman 1993; Petit et al. 2018). The black solid (dashed) lines are the network of first-order (second-order) two-body mean motion resonances. The bold solid black diagonal line is the locus of equal orbital period ratios (main diagonal). The oblique green lines represent the three-body resonance network for $p + q < 30$. The bold green lines is the loci of the three-body resonances for $\alpha = q/p = 1/2; 2/3; 1; 3/2; 2$. The blue curve is the theoretical overlap limit as defined by PPDJ20 for Earth-mass planets. The black square contains the area of investigation of the study, which spans inverse period ratio values between ~ 0.90 and ~ 0.94 .

6. Dynamics of Anomalously Long-Lived Systems

6.1. Spikes SPK4 and SPK5

Figure 2 does not show any straightforward correlations between the lifetime of the spike systems and the initial angles in the case of SPK4 and SPK5. Paper I did find a correlation between initial angular orbital elements and the survivability of spike systems with $\beta > 5$. Rather than further increasing the resolution in β in the Random set around the spikes, we can improve the statistics by exploring the dependence of initial angles on the survivability for a selection of systems in SPK4 and SPK5. We select the first survivor ($t_c/t_0 \geq 10^{10}$ years) in SPK4, i.e., the system with initial $\beta = 5.1547$ (hereafter called b515), as well as the system with initial $\beta = 5.4135$ (hereafter called b541). These systems have initial inverse period ratios of 0.9068 and 0.9023, respectively.

We first test the lifetime dependence of SPK5 on the initial longitudes by exploring the lifetime of system b541 for different sets of initial angles (λ_2 and λ_3). Because SPK5 is located in a dip (see Fig. 1), we know that the non-long-lived systems will be short-lived (the dip goes down to 2σ below the exponential fit at b541, which corresponds to $t_c/t_0 \approx 4000$ yrs). We can therefore consider a relatively high resolution in initial angles while keeping the total integration time relatively short. We choose a resolution of 1° in initial longitude from 0 to 359° .

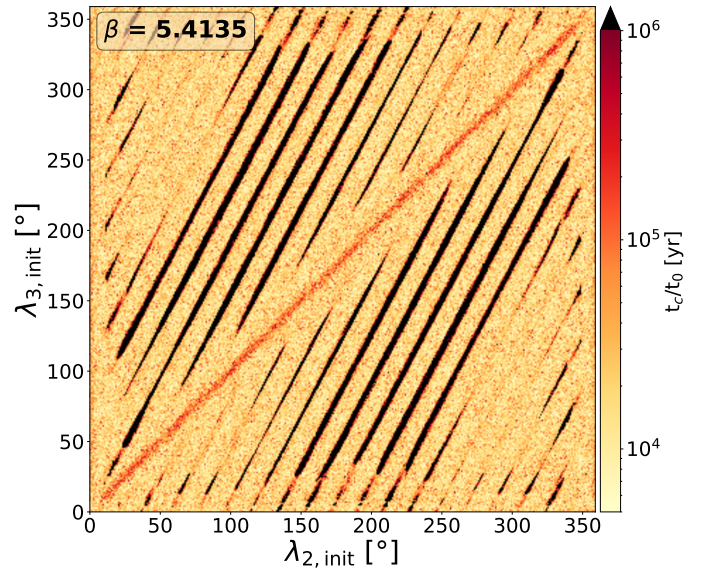


Fig. 7: Systems' lifetimes as a function of the initial longitudes of the middle planet (λ_2) and outer planet (λ_3). The value of initial orbital separation $\beta = 5.4135$ was selected from SPK5, where our Random integration with initial longitudes $\lambda_2 = 228.228024^\circ$ and $\lambda_3 = 145.726985^\circ$ had a lifetime $> 10^{10}$ years. The grid's resolution is 1° , and it extends over the entire range, yielding $360 \times 360 = 129,600$ simulations. The integrations were halted after 10^6 yrs, with a total of 12,001 runs reaching this time limit. These systems are shown in black.

The resulting grid is shown in Figure 7, where we see a clear pattern consisting of successive stripes of long-lived systems. The stripes show gaps near the initial configuration $\lambda_2 = \lambda_3$, reflecting strong asymmetric perturbations between planets 2 and 3 at the onset of the integration.

By setting the initial angle $\lambda_1 = 0^\circ$, we can rearrange Eq. 8 and express λ_3 as a function of λ_2 :

$$\lambda_3 = \frac{p+q}{q} \lambda_2 + \frac{\phi}{q}, \quad (14)$$

which represents the equation of a straight line of slope $(p+q)/q$ passing through the point $(\phi/q, \phi/q)$. If we assume that the stripes are the result of a three-body resonance, then Eq. 14 tells us that the number of stripes (counting from $\lambda_2 = 0^\circ$ to 360°) is given by the index of the resonance $p+q$ and the slope of the stripes by $(p+q)/q$. We count 19 stripes from Fig. 7, meaning that $p+q = 19$. Considering that the slope appears to be slightly less than 2 and that 19 is an odd number, it is very likely that $q = p+1$. This should therefore be the result of the zeroth-order 3BR with $\alpha = 10/9$.

We can trivially verify this assumption by checking if the stable systems cluster around a given angle ϕ for $3\text{BR}\alpha 10/9$. Figure 8 shows that all long-lived systems unambiguously cluster around the resonant angle $-19\lambda_2 + 10\lambda_3 = 0^\circ$. In Figure 9, we compare the map of ϕ for all values of angles with the lifetime grid for b541. The long-lived stripes clearly overlap with the locations where $\phi = 0^\circ$, meaning that the dynamics of system b541 is driven by $3\text{BR}\alpha 10/9$.

We can apply the same analysis for the system b515. However, unlike b541, SPK4 is not in a dip (Fig. 1). Instead, most systems in the vicinity of SPK4 have lifetimes of about 2σ above the exponential fit, corresponding to $t_c/t_0 \approx 10^5$ yrs at location

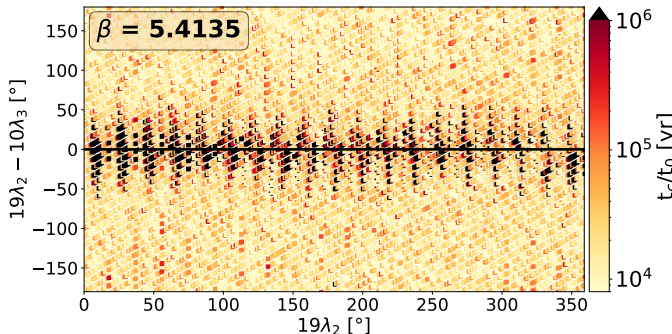


Fig. 8: Lifetimes of systems $b541$ (dataset from Fig. 7), distributed in the three-body resonance space with $\alpha = 10/9$. The long-lived systems cluster around the resonant angle $\phi = 0^\circ$. Systems that survived for more than 10^6 yrs are shown in black.

of $b515$, which would make the computation of a grid similar to Fig. 7 significantly more costly. We draw 2000 systems $b515$ from a random distribution of initial angles λ_2 and λ_3 and check for which pair of p, q values the long-lived systems cluster around an angle ϕ . As seen in Figure 10, we find that the $b515$ systems cluster around $\phi = 180^\circ$ for the pair $\alpha = 11/10$.

To illustrate this, we show the trajectories of the two systems $b515$ and $b541$ in Figure 11. In this region, the 3BR network is really dense, and the width of the two resonances overlaps. However, there is no noticeable diffusion on the plane during the whole integration (up to 10^{10} yrs) and the two systems remain away from the 2BR network (of first- and second-order 2BRs). Note that all spike systems observed in Paper I are also found away from 2BRs (whereas dips are in the vicinity of 2BRs). For comparison, we show the trajectory of a system midway between $b515$ and $b541$. This system starts to diffuse perpendicular to the 3BR network (as expected by Chirikov diffusion) within the first few thousands of orbits.

6.2. Spikes SPK1, SPK2, SPK3

In Fig. 2, we saw an excess of long-lived systems with the outer pair of planets initially close to conjunction. This result should be approached with caution because integrations that start close to conjunctions begin with a highly-asymmetric transfer of energy and angular momentum from the planet closer to the star (in this case, the middle planet of the system) to the one farther out, producing a wider separation between the orbits of these two planets (and, provided the innermost planet in the system starts far from alignment, a reduction in the separation of the inner pair of planets by about half as much), effectively moving the system away from equal initial period ratios. The system is thus "pushed" toward the lower right in the period ratio plane.

We select one representative system from each of SPK1, SPK2, and SPK3. For SPK1, we use the last on the survivors list ($t_c/t_0 \geq 10^{10}$ years) from Specific Set 1, the system with initial $\beta = 3.82086$ (hereafter called $b382$). For the other spikes, we select the longest-lived system in each spike of the Standard Random set, that is, $\beta = 4.15423$ and $\beta = 4.51276$, hereafter called $b415$ and $b451$, for SPK2 and SPK3, respectively. All three of these systems have outer pairs initially near conjunction. Figure 12 shows the trajectory of these three systems over the first 100 years. Showing the trajectory allows one to visualize the effects of conjunctions, which draw "wings" on the plane. The lower right wings are the effect of inner pair conjunctions, and the up-

per left wings are due to the conjunctions of the outer pair. We see that the integrator interprets the initial conjunction as the second half of an outer pair conjunction of another system¹. Typically, for very low eccentricities, the interaction is symmetric, so the exchange of orbital energy cancels out; the system goes back to its initial position in the 2-D plane after the conjunction. However, if only half of the interaction is considered, then the exchange of energy is not canceled out, and the system goes in a wrong direction. In this case, long-lived systems are interpreted as systems located in the vicinity of the isolated $3BR\alpha 1$. The fact that these systems are stable is thus only due to the fortuitous proximity of this resonance. Note that similar numerical studies using random initial longitudes also have a fraction of systems with pairs of planets initially close to conjunctions, but most of these studies focused on systems with more than three planets, where groups of three resonant planets are likely to be destabilized by perturbations from other planets.

To illustrate the dynamics with respect to $3BR\alpha 1$, in Figure 13 we show the evolution of the resonant angle over the first 1000 years. The system $b415$ librates around the resonant angle $(-2\lambda_2 + \lambda_3 = 180^\circ)$, whereas the system $b451$ circulates, which is expected as the system settled just outside of $3BR\alpha 1$. The resonant angle for $b382$ appears to librate around $-2\lambda_2 + \lambda_3 = 192.57^\circ$ with a very small amplitude and without a clear periodic pattern. None of these systems experiences a triplet close encounter during the first 1000 years. (Moreover, the system $b382$ does not experience any triplet close encounters during the total integration time of 10^{10} yrs. Thus, the system remains effectively locked in this 3BR during the whole integration.) Note that not experiencing triplet close encounters is not a requirement for stability. The two systems $b382$ and $b415$ are also in the vicinity of the intersection of two second-order 2BRs, (27:29 and 25:27 for $b382$, and 25:27 and 23:25 for $b415$), but none of these two-body resonant angles librates (not shown), meaning that both systems are locked in a true 3BR (Papaloizou 2015; Goździewski et al. 2016). The system $\beta = 3.4744$ of the S2 set also librates around $-2\lambda_2 + \lambda_3 \approx 150^\circ$. Unlike SPK4 and SPK5, all systems discussed here (SPK1, SPK2, SPK3) remain in the vicinity of 2BR intersections (see Appendix C).

Figure 14 shows, for the case of $b382$, the results of an analysis similar to that in Sect. 6.1 and Fig. 7. Interpreting the result is not as straightforward as in the case of $b541$. The surface shows 13 successive small long-lived islands along the diagonal $\lambda_2 = \lambda_3$, as well as a succession of faint stripes throughout the surface. There should be 14 stripes passing through the long-lived islands. If we follow the same analysis as in Sect. 6.1, we find $p + q = 14$, such that $\alpha = 4/3$ or $\alpha = 1$. However, we know from Figs. 12 and 13 that the dynamics is, at least partially, regulated by the $3BR\alpha 1$, and therefore $\alpha = 4/3$ shall be excluded. Since only the close-to-conjunction initial configurations can push the system toward $3BR\alpha 1$, the long-lived resonant systems are necessarily in the vicinity of the line $\lambda_2 = \lambda_3$, and the small long-lived islands in Fig. 14 are the parts of the 14 stripes that lie in the vicinity of the $\lambda_2 = \lambda_3$ diagonal. In Appendix A, we show the same figure in the case of a system that starts directly on $3BR\alpha 1$.

6.3. The wide region between spikes

As mentioned in Sect. 3.1, there is a wide region without any spikes between SPK3 and SPK4. In Sect. 6.2, we saw that

¹ For this reason, authors usually choose to initialize integrations of systems far from conjunctions (see, e.g., Smith & Lissauer 2009).

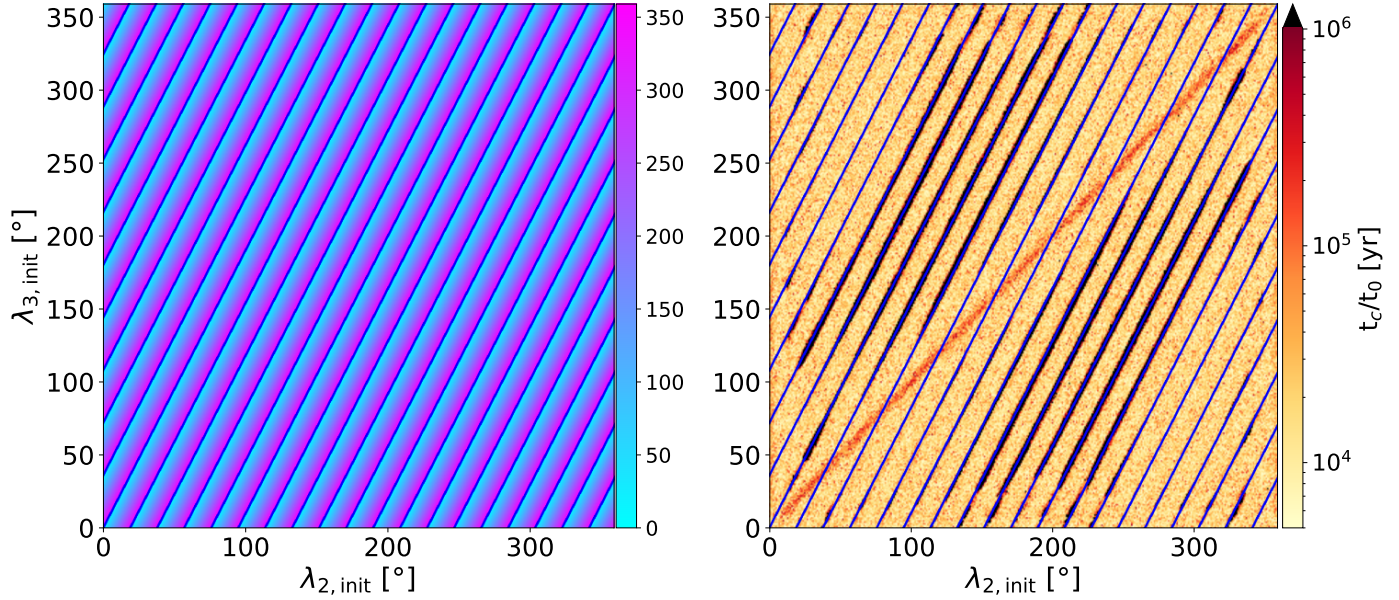


Fig. 9: Left: resonant angle ϕ with $\alpha = 10/9$ for all values of angles λ_2 and λ_3 . The dark blue stripes correspond to $\phi = 0^\circ$. Right: Same as Fig. 7, but with the blue stripes overlaid on top. The angle $\phi = 0^\circ$ overlaps with the stripes of long-lived systems.

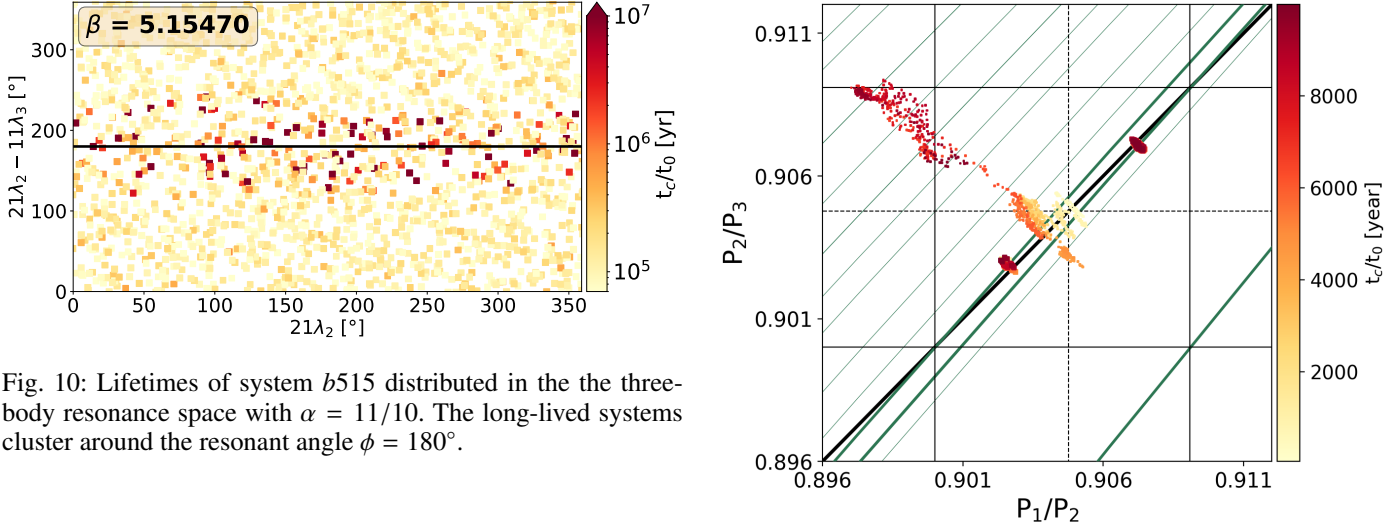


Fig. 10: Lifetimes of system $b515$ distributed in the three-body resonance space with $\alpha = 11/10$. The long-lived systems cluster around the resonant angle $\phi = 180^\circ$.

the systems are "pushed" towards the 3BR $\alpha 1$ where they remain locked in a stable configuration. Furthermore, we saw that 3BR $\alpha 1$ is special (Sect. 5) as it is the most isolated resonance of the 3BR network. In Fig. 12, the green shaded area represents the width of the resonance as defined by PPDJ20 (their Eq. 55). Because 3BR $\alpha 1$ is located on the lower right side of the diagonal, the systems starting on the main diagonal with the outer pair initially close to conjunction can be captured by this resonance (see Sect. 6.2).

The distance in the period-ratio plane to which a system can be "pushed" due to a conjunction depends on the initial orbital spacings. If the initial orbital spacing is too large, then the energy exchange during the two-planet conjunction cannot allow the systems to reach the vicinity of the resonance. We see from Fig. 12 that the system in SPK3 barely made it to the resonance width, suggesting that there cannot be other spikes due to this resonance for larger β values. In this sense, SPK3 is a transition spike. The next spikes (SPK4, SPK5, and further) can only be the result of a capture by a 3BR that intersects the main diagonal.

Fig. 11: Trajectory over the first 10,000 years, with a moving average of 20 years, in the period-ratio plane for three selected systems, one in SPK4 ($\beta = 5.1547$), one in SPK5 ($\beta = 5.4135$), and one midway in the vicinity of a second-order 2BR intersection ($\beta = 5.2813$), with the same initial longitudes as the system in SPK4.. The black vertical and horizontal solid and dashed lines correspond to first and second order two-body MMRs, respectively, between adjacent pairs of planets. The solid black diagonal line in the upper right corner is the first order MMRs between the inner and outer planets. The green oblique lines correspond to the zeroth-order three-planet MMRs. Only the 3BRs with $p + q < 24$ are shown. The three bold green curves correspond to 3BRs with, from left to right, $\alpha = 11/10$, $\alpha = 10/9$, and $\alpha = 1$.

7. Unequally-Spaced Initial Orbits

In Sect. 6.2, we showed that the long-lived systems of the inner spikes possess non-uniform proper elements. However, this

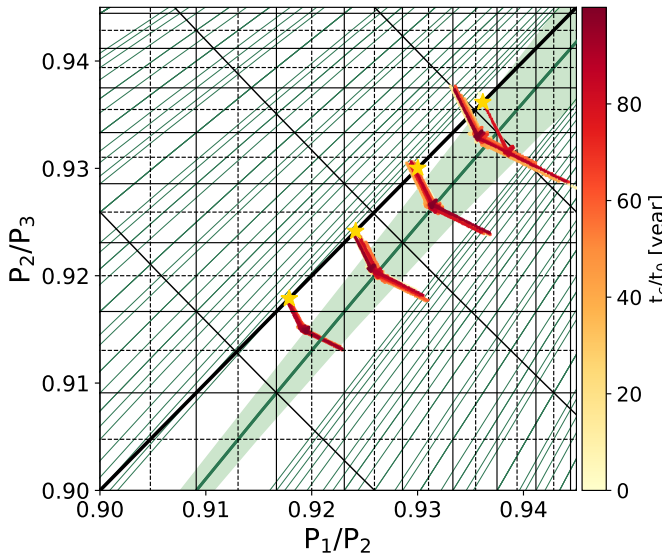


Fig. 12: Trajectory over the first 100 years in the period-ratio plane for three selected systems in SPK1 ($\beta = 3.82086$, $\lambda_2 = 166.273784^\circ$, $\lambda_3 = 165.110014^\circ$), SPK2 ($\beta = 4.15423$, $\lambda_2 = 179.01980^\circ$, $\lambda_3 = 178.62^\circ$), and SPK3 ($\beta = 4.51276$, $\lambda_2 = 211.95^\circ$, $\lambda_3 = 212.22^\circ$). We also show, for comparison, the trajectory of the longest-lived very closely-spaced system in S2 set ($\beta = 3.4744$, $\lambda_2 = 207.16381^\circ$, $\lambda_3 = 208.66160^\circ$), which is located near the upper right corner. Positions are drawn every 0.1 years. The gold stars represent the period ratios at start of integration. The solid black and dashed lines correspond to first and second order two-body MMRs, respectively. The solid bold black diagonal is the location of equally-spaced orbits (the main diagonal). The green oblique lines correspond to the loci of the zeroth-order three-planet MMRs for $p + q < 24$. The shaded green area is the width (Eq. 55 of PPDJ20) of the resonance with $\alpha = 1$.

should not invalidate the fact that these systems are, in fact, stable; they simply do not belong to the "proper" main diagonal. This justifies further numerical investigations and requires performing integrations of systems outside the main diagonal, i.e., systems with non-evenly spaced orbits. In this section, we will focus on the 3BR α 1.

Because 3BR α 1 is the most isolated 3BR, the stability of the systems locked on this 3BR is mainly regulated by the position relative to the 2BR network. We saw in Sect. 5 that the 3BR α 1 systematically passes through intersections of 2BRs of the same order. Therefore, both pairs of a triplet located on top of the 3BR α 1 always have the same dynamical behavior. Successive conjunctions of planet pairs in first-order 2BRs occur for initial configuration in the same longitude in inertial frame apart from (usually small) corrections to account for apse precession, while for second-order 2BRs successive configurations occur near opposite longitude in inertial frame (Murray & Dermott 1999). This can have a cancellation effect for high-order 2BRs and eccentric orbits (e.g., Peale 1976; Tamayo & Hadden 2025). This dynamical behavior is transferred to the 3BR lying at the intersection of the two k th-order 2BRs. More precisely, if a system locked in the 3BR α 1 is at the intersection of two k th-order 2BRs, then the triplet goes back to its initial configuration in the same longitude in inertial frame every $k \times P_{3\text{br}}$. Thus, similarly to two-body conjunctions in two-planet systems, canceling effects from conjunctions in a three-planet system can increase

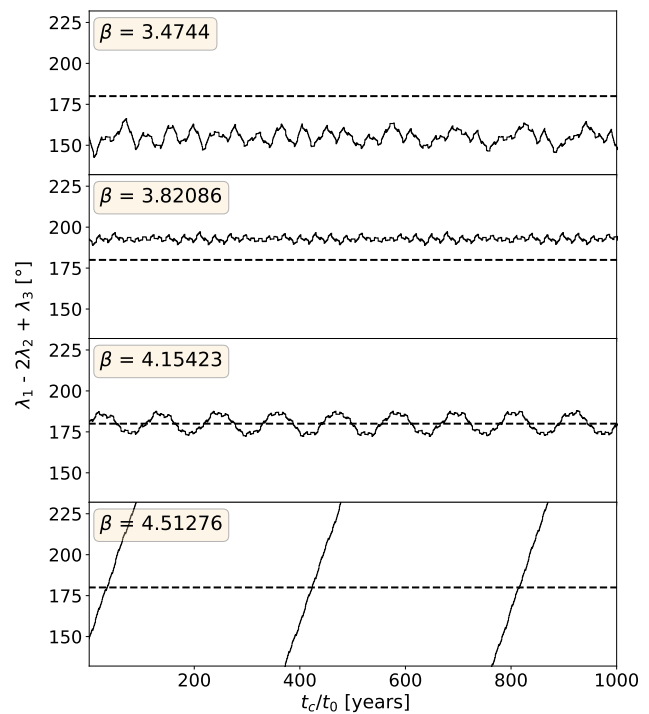


Fig. 13: Evolution of three-body resonant angles over the first 1000 orbits of four systems. The upper panel shows the (relatively) long-lived, extremely closely-spaced, system in S2 set ($\beta = 3.4744$, $\lambda_2 = 207.16381^\circ$, $\lambda_3 = 208.66160^\circ$). The second panel shows the system in SPK1 ($\beta = 3.82086$, $\lambda_2 = 166.273784^\circ$, $\lambda_3 = 165.110014^\circ$), the third panel show the system in SPK2 ($\beta = 4.15423$, $\lambda_2 = 179.02^\circ$, $\lambda_3 = 178.62^\circ$), and the bottom panel SPK3 ($\beta = 4.51276$, $\lambda_2 = 211.95^\circ$, $\lambda_3 = 212.22^\circ$).

the system's stability with favorable longitudes of periapsis (but this is beyond the scope of this paper).

With that in mind, we can speculate and predict the lifetime pattern on the period-ratio plane for systems that are initially in the vicinity of the 3BR α 1. A first-order 2BR has a tendency to excite the eccentricities, increasing the period ratios of the planet pair. This explains why for equally spaced systems, the dips in lifetime are always located just narrow of first-order resonances (Lissauer & Espresate 1998; Espresate & Lissauer 2001; Obertas et al. 2017; Lissauer & Gavino 2021; Lammers et al. 2024). A system on top or slightly outside (more widely-spaced than) the crossing point of two first-order 2BRs diffuses parallel to the main diagonal (roughly parallel to the 3BR α 1 itself) in regions where period ratios are close to 1) and remains safe from Chirikov diffusion. We can therefore expect to see stable islands located outside the intersection of two first-order 2BRs. On the other hand, because the strength of second-order 2BRs is proportional to the eccentricities, which are all initially zero in this study, the systems simply stay on the 3BR α 1 and can become secularly stable (with the right set of longitudes). Stable islands should be located directly on top of the intersection of two second-order two-body MMRs.

We use Eq. 3 to define two different orbital separations, one for the inner pair β_{12} and another for the outer pair β_{23} , and derive

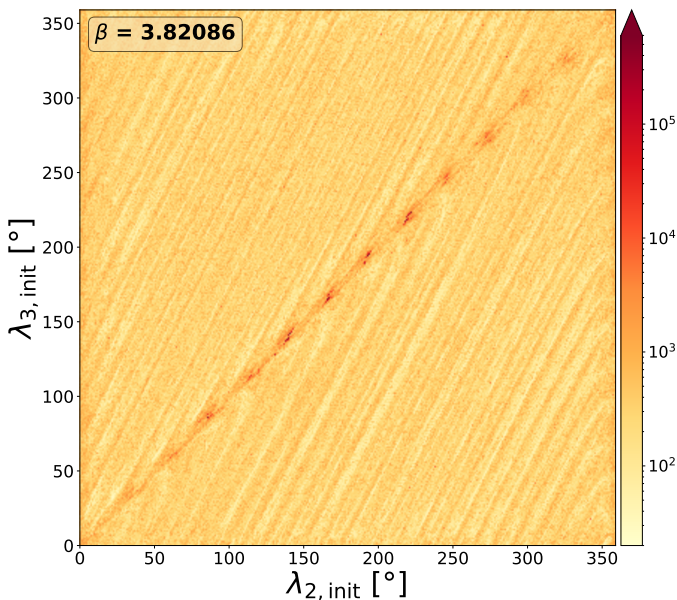


Fig. 14: System's lifetime as a function of the initial longitudes of the middle (λ_2) and outer planet (λ_3). The system has an initial $\beta = 3.82086$, selected from the spike in Specific Set S1 with a lifetime of 10^{10} years. The resolution in angle is 1° , i.e., a total of 360×360 integrations.

the initial orbital elements accordingly. To limit the computation time, we choose to restrict the integrations in a small surface of the period-ratio plane ranging from the Hill stability limit to $\beta_{12} + \beta_{23} = 10$, which corresponds to the shape of a triangle in the (β_{12}, β_{23}) plane, and we stop the integration if the system remains stable for at least 10^7 years. We choose a single, widely-spaced set of initial longitudes $\lambda_2 = 222.49^\circ$ and $\lambda_3 = 84.98^\circ$, which were used by [Smith & Lissauer \(2009\)](#) and are the “SL09” set used by [Paper I](#). All integrations thus start far from any planet conjunctions, and this set is such that $3BR\alpha 1$ has a value $\phi = 0^\circ$.

The numerical results are shown in Figure 15, where we see the presence of a grid of (relatively) stable islands, with a typical lifetime between 5,000-10,000 yrs. This grid of quasi-stable islands is a direct consequence of the 2BR network, as suggested above. The additional presence of anomalously long-lived islands strikes immediately. These particular islands, which also follow the overall 2BR grid pattern, are due to the 3BR network. We can see that these long-lived islands are systematically in the vicinity of well-isolated 3BRs. In particular, there is the predicted chain of very long-lived islands along the $3BR\alpha 1$. It consists of a succession of small long-lived islands lying on top of the intersection of second-order 2BRs, and larger long-lived islands directly outside the intersection of first-order 2BRs. These islands appear to be confined and shaped by the 3BR network (this is also true for the other long-lived islands on top of other 3BRs). This confinement means that the locations where the systems can be stable are regulated by 2BRs, while the protection of well-isolated 3BRs allows the systems to become anomalously long-lived, up to 10^{10} years (see Fig. 4), even in regions very close to the Hill stability limit and well within the overlap stability limit of 3BRs.

8. Discussion

Figure 15 illustrates why extremely closely-spaced three-planet systems are more likely to be stable in the vicinity of an iso-

lated 3BR. Here, we briefly discuss the known closely-spaced *Kepler* systems with at least three planets and their position on the 3BR network, in particular around the isolated $3BR\alpha 1$, $3BR\alpha 3/2$, and $3BR\alpha 2$. As mentioned in Sect. 5, these three resonances are those with the highest number of resonances lying on top of each other, which is correlated with the density of 2BRs intersection crossings and their isolation from the rest of the 3BR network.

Figure 16 shows triplets of tightly-spaced *Kepler* planets on the period-ratio plane. Among them are notable tightly-spaced chains of resonances and planet triplets known to be captured in 3BRs. The system Kepler-60 ([Steffen et al. 2013](#); [Goździewski et al. 2016](#); [Jontof-Hutter et al. 2016](#)), hosts a triplet that lies on the $3BR\alpha 1$ as well as in the vicinity of the intersection of two first-order 2BRs (4:5 and 3:4) (e.g. [Goździewski et al. 2016](#)). Kepler-223 has four confirmed planets ([Lissauer et al. 2014](#); [Rowe et al. 2014](#); [Mills et al. 2016](#)) and therefore two consecutive triplets. Both triplets lie on the main 3BRs ($\alpha 1$ for the inner triplet and $\alpha 2$ for the outer triplet) and each adjacent pair is also on top of a first-order 2BR (3:4, 2:3, 3:4).

Kepler-11 ([Lissauer et al. 2011a](#)), Kepler-80 ([Lissauer et al. 2011b](#); [Shallue & Vanderburg 2018](#); [MacDonald et al. 2021](#)), Kepler-102, and Kepler-90 are the only *Kepler* systems with six planets where at least two triplets are represented on Fig. 16. The triplet positions on the period-ratio plane are fundamentally different between these systems. Kepler-80 is one of the most notable cases of resonant chains ([MacDonald et al. 2016, 2021](#)) where all triplets among the five planets in the chain are lying near the main isolated 3BRs: $3BR\alpha 1$, $3BR\alpha 2$, $3BR\alpha 3/2$, and for the innermost triplet, the middle triplet, and the outermost triplet, respectively. On the other hand, Kepler-11’s triplets are scattered away from the main isolated 3BRs. Kepler-102 is the only six-planet system with four triplets visible, i.e., with all adjacent pairs having period ratios > 0.58 . Two of them are in the direct vicinity of $3BR\alpha 2$, one in the vicinity of $3BR\alpha 1$, and another away from any 2BRs and isolated 3BRs. These systems have very closely-packed adjacent planets, with similar values of period ratios, but exhibit very different architectures, which is commonly attributed to different formation mechanisms (e.g., [Hands et al. 2014](#)). Note that most *Kepler* planets have mass ratio to their star that is a factor of $\sim 2-8$ times as large as what we simulated in this paper, but there are some *Kepler* planets with substantially smaller masses. Figure 16 also shows the position of the adjacent triplets in TRAPPIST-1 ([Gillon et al. 2017](#); [Luger et al. 2017](#); [Agol et al. 2021](#)). Similarly to the *Kepler* resonant triplets, all adjacent ones in TRAPPIST-1 are on top of the main isolated 3BRs, as well as in the vicinity of first-, second-, and third-order 2BR intersections.

More globally, [Cerioni et al. \(2022\)](#), using a statistical analysis, found a correlation between the observed distribution of planet triplets and the main isolated 3BRs. The fact that most of the very tightly-packed resonance chains observed are in the vicinity of the main isolated 3BRs suggests that these resonances are more fundamental than the 2BR network (in this area of the period ratio plane), and the results shown in Fig. 15 is a direct demonstration that the stability of very tightly-packed resonant systems cannot be understood without addressing the interplay between the 2BR network and the 3BR network, a mechanism that is to be included as features in stability prediction models (e.g. [Tamayo et al. 2016](#); [Thadhani et al. 2025](#)). The extremely tightly-packed resonant chains are expected to be located on these isolated 3BRs because they represent the only locations on the period ratio plane protected from Chirikov diffusion (for

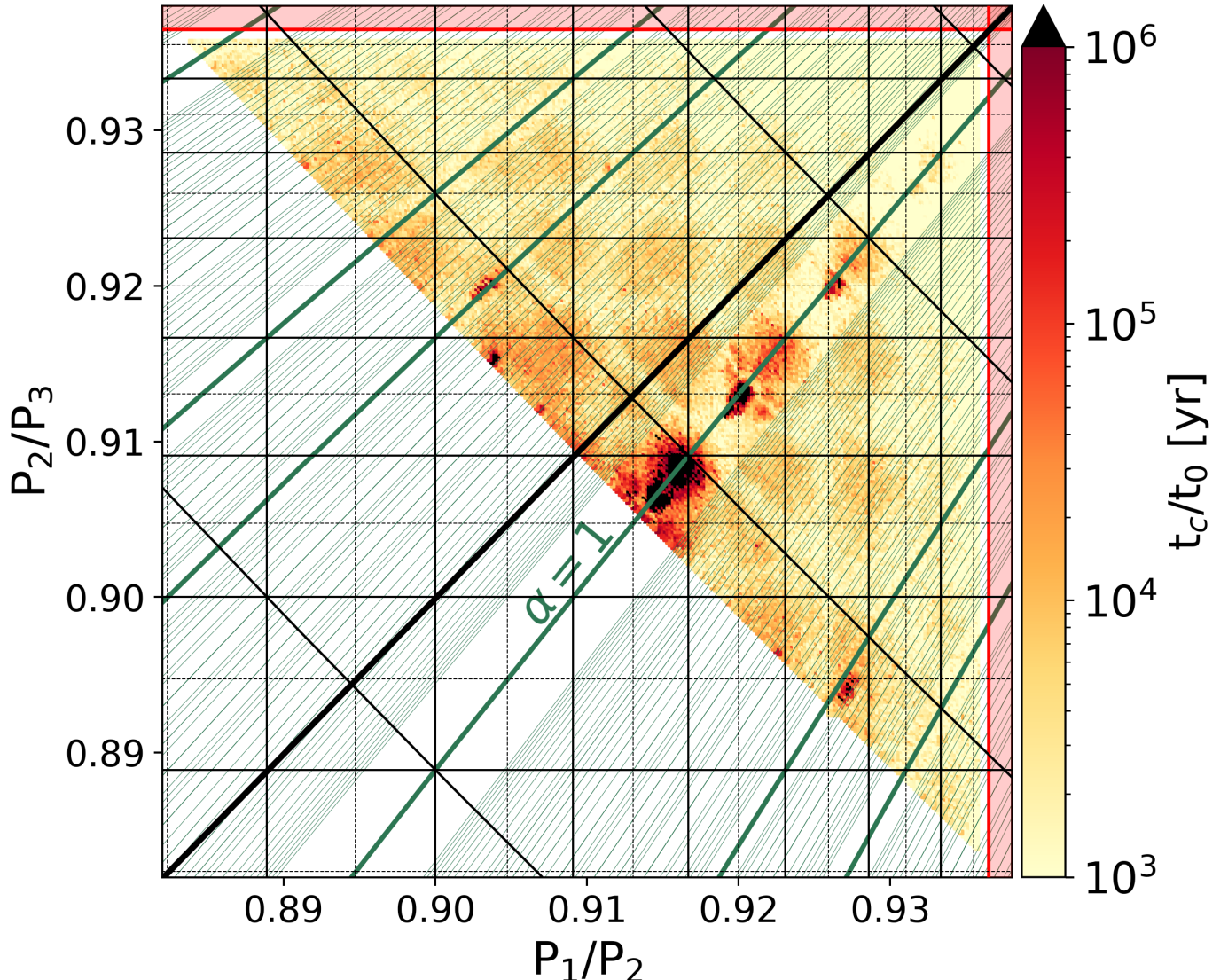


Fig. 15: Lifetime (color-map) of systems with unevenly-spaced orbits shown in the period-ratio plane. Integrations are performed over a surface ranging from the Hill stability limit to $\beta_{12} + \beta_{23} = 10$. The resolution in P_j/P_{j+1} is $\sim 1.90 \times 10^{-4}$ (or 0.01 in β). The initial set of longitudes is $\lambda_2 = 222.49^\circ$ and $\lambda_3 = 84.98^\circ$, same as in [Smith & Lissauer \(2009\)](#) and [Paper I](#), and correspond to a resonant angle $-2\lambda_2 + \lambda_3 \approx 0^\circ$. The black diagonal represents systems with evenly-spaced orbits, and the oblique green lines represent the network of three-body commensurability. The bold green lines are resonances in less dense regions, including 3BR α 1 and 3BR α 3/2 in the upper left. In the vicinity of 3BR α 1, 276 systems survived for more than 10^6 years, including 60 systems that survived for more than 10^7 years. Elsewhere (other isolated islands), 19 systems survived for more than 10^6 years and 0 for more than 10^7 years. Systems with a lifetime greater than 10^6 years are represented in black.

period ratios close to 1, a system can diffuse roughly parallel to the 3BR network only if it is captured by these resonances).

9. Conclusions

We use numerical simulations to investigate the dynamics of extremely compact three-planet systems ($P_j/P_{j+1} \gtrsim 0.90$ or $\beta \lesssim 5.6$). Our study shows that there is a small set of initial conditions for which three-planet systems that are more tightly-packed than any systems observed thus far can remain dynamically stable for billions of orbits. In light of previous analytical studies (e.g., [Quillen 2011](#); [Petit et al. 2020](#)) and of observed systems, we present a qualitative analysis of the role of three-body resonances and the relationship between their initial longitudes.

First, we argue that the most isolated three-body resonances, most specifically 3BR α 2/3, 3BR α 1, 3BR α 3/2, and 3BR α 2, are favorable locations for stabilizing extremely tightly packed three-planet systems. Second, we show that the overall stability depends on the interplay between these isolated three-body resonances and the surrounding two-body resonance network. We can summarize the results as follows:

- In numerical simulations, we observe the presence of anomalously very stable systems with extremely small period ratios that can remain stable over very long times. We show that this stability is correlated with the initial longitudes.
- The stability's dependence on initial longitudes reflects the capture into a three-body resonance. Extremely compact three-planet systems can remain stable only if their dynamics

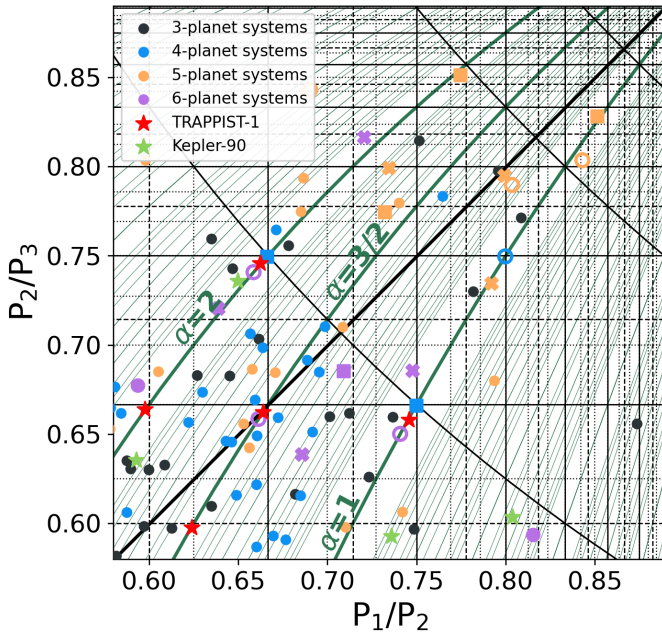


Fig. 16: Period-ratio plane with triplets of adjacent planets in *Kepler* systems in the region $0.58 < P_j/P_{j+1} < 0.90$ (Lissauer et al. 2024). The black markers show the position of triplets of planets inside three-planet systems. The blue markers show triplets inside four-planet systems (up to two markers per system) where the empty circles, and squares represent the triplets in Kepler-60 and Kepler-223, respectively. The yellow markers show triplets in five-planet systems (up to three markers per system) where the empty circles, squares, and crosses represent the triplets in Kepler-1371 and Kepler-1542, and Kepler-444, respectively, and the purple markers show the triplets in six-planet systems (up to four markers per system) where the empty circles, squares, and crosses represent the triplets in Kepler-80, Kepler-11, and Kepler-102, respectively. The triplets in the eight-planet system Kepler-90 are shown by the light green stars. For comparison, the red stars show the successive triplets in the TRAPPIST-1 system. The solid, dashed, and dotted black lines are the first-order, second-order, and third-order two-body mean motion resonances, respectively. The oblique green lines are the zeroth-order three-body mean motion resonances, where the bold green ones represent resonances with $\alpha = 1$, $\alpha = 2$, and $\alpha = 3/2$, which are the three most isolated three-body resonances in the vicinity of the main diagonal.

is regulated by three-body resonances, in particular a specific subset of resonances.

- Some three-body resonances are more isolated than others in the network. We show that the degree of isolation of a three-body resonance is regulated by the two-body resonance network; the three-body resonances cross intersections of two-body resonances and the degree of isolation is proportional to the density of intersection crossings, which depends on the ratio $\alpha \equiv q/p$. The most isolated three-body resonances are the ones with $\alpha = 1/2; 2/3; 1; 3/2; 2$. We leave this question for future work.
- This isolation is the main protection against chaotic diffusion in the case of extremely tightly-packed three planets systems, those that lie inside the three-body resonance overlap limit, and more specifically for those with $P_j/P_{j+1} > 0.90$. These extremely tightly-packed stable triplet of planets similar in

size or larger than Earth, if observed, are therefore expected to be located near this subset of the three-body resonance network.

Acknowledgements. We thank Antoine Petit, Tjarda Boekholt, and Dan Sirbu for crucial discussions. S.G. acknowledges support from the ERC Synergy Grant “ECOGAL” (project ID 855130) and the Independent Research Fund Denmark (grant No. 0135-00123B).

References

Agol, E., Dorn, C., Grimm, S. L., et al. 2021, PSJ, 2, 1
 Aksnes, K. 1988, in Long-term Dynamical Behaviour of Natural and Artificial N-body Systems, ed. A. D. Roy, 125–139
 Bartram, P., Wittig, A., Lissauer, J. J., Gavino, S., & Urrutxua, H. 2021, MNRAS, 506, 6181
 Batygin, K. & Adams, F. C. 2017, AJ, 153, 120
 Cerioni, M., Beaugé, C., & Gallardo, T. 2022, MNRAS, 513, 541
 Chambers, J. E. 1999, MNRAS, 304, 793
 Chambers, J. E., Wetherill, G. W., & Boss, A. P. 1996, Icarus, 119, 261
 Chirikov, B. V. 1979, Phys. Rep., 52, 263
 Dai, F., Goldberg, M., Batygin, K., et al. 2024, AJ, 168, 239
 Deck, K. M., Payne, M., & Holman, M. J. 2013, ApJ, 774, 129
 Espa駉te, J. & Lissauer, J. J. 2001, Icarus, 152, 29
 Fabrycky, D. C., Lissauer, J. J., Ragozzine, D., et al. 2014, ApJ, 790, 146
 Gillon, M., Triaud, A. H. M. J., Demory, B.-O., et al. 2017, Nature, 542, 456
 Gladman, B. 1993, Icarus, 106, 247
 Goldberg, M. & Batygin, K. 2022, AJ, 163, 201
 Go  dziewski, K., Migaszewski, C., Panichi, F., & Szuszkiewicz, E. 2016, MNRAS, 455, L104
 Gratia, P. & Lissauer, J. J. 2021, Icarus, 358, 114038
 Hadden, S. & Lithwick, Y. 2018, AJ, 156, 95
 Hands, T. O., Alexander, R. D., & Dehnen, W. 2014, MNRAS, 445, 749
 Hill, G. W. 1878, American Journal of Mathematics, 1, 5
 Izidoro, A., Bitsch, B., Raymond, S. N., et al. 2021, A&A, 650, A152
 Izidoro, A., Ogihara, M., Raymond, S. N., et al. 2017, MNRAS, 470, 1750
 Jontof-Hutter, D., Ford, E. B., Rowe, J. F., et al. 2016, ApJ, 820, 39
 Lammers, C., Hadden, S., & Murray, N. 2024, ApJ, 972, 53
 Lissauer, J. J. & Espa駉te, J. 1998, Icarus, 134, 155
 Lissauer, J. J., Fabrycky, D. C., Ford, E. B., et al. 2011a, Nature, 470, 53
 Lissauer, J. J. & Gavino, S. 2021, Icarus, 364, 114470
 Lissauer, J. J., Marcy, G. W., Bryson, S. T., et al. 2014, ApJ, 784, 44
 Lissauer, J. J., Ragozzine, D., Fabrycky, D. C., et al. 2011b, ApJS, 197, 8
 Lissauer, J. J., Rowe, J. F., Jontof-Hutter, D., et al. 2024, PSJ, 5, 152
 Luger, R., Sestovic, M., Kruse, E., et al. 2017, Nature Astronomy, 1, 0129
 MacDonald, M. G., Ragozzine, D., Fabrycky, D. C., et al. 2016, AJ, 152, 105
 MacDonald, M. G., Shakespeare, C. J., & Ragozzine, D. 2021, AJ, 162, 114
 Millholland, S., Wang, S., & Laughlin, G. 2017, ApJ, 849, L33
 Mills, S. M., Fabrycky, D. C., Migaszewski, C., et al. 2016, Nature, 533, 509
 Morrison, S. J. & Kratter, K. M. 2016, ApJ, 823, 118
 Murray, C. D. & Dermott, S. F. 1999, Solar System Dynamics
 Obertas, A., Van Laerhoven, C., & Tamayo, D. 2017, Icarus, 293, 52
 Outland, B., Noble, G., Smith, A. W., & Lissauer, J. J. 2026, arXiv e-prints, arXiv:2601.11692
 Papaloizou, J. C. B. 2015, International Journal of Astrobiology, 14, 291
 Peale, S. J. 1976, ARA&A, 14, 215
 Petit, A. C. 2021, Celestial Mechanics and Dynamical Astronomy, 133, 39
 Petit, A. C., Laskar, J., & Bou  , G. 2018, A&A, 617, A93
 Petit, A. C., Pichierri, G., Davies, M. B., & Johansen, A. 2020, A&A, 641, A176
 Pichierri, G. & Morbidelli, A. 2020, MNRAS, 494, 4950
 Quarles, B. & Lissauer, J. J. 2018, AJ, 155, 130
 Quillen, A. C. 2011, MNRAS, 418, 1043
 Rein, H. & Liu, S. F. 2012, A&A, 537, A128
 Rein, H. & Tamayo, D. 2015, MNRAS, 452, 376
 Rice, D. R. & Steffen, J. H. 2023, MNRAS, 520, 4057
 Rowe, J. F., Bryson, S. T., Marcy, G. W., et al. 2014, ApJ, 784, 45
 Shalh, C. J. & Vanderburg, A. 2018, AJ, 155, 94
 Smith, A. W. & Lissauer, J. J. 2009, Icarus, 201, 381
 Smith, A. W. & Lissauer, J. J. 2010, Celestial Mechanics and Dynamical Astronomy, 107, 487
 Steffen, J. H., Fabrycky, D. C., Agol, E., et al. 2013, MNRAS, 428, 1077
 Tamayo, D. & Hadden, S. 2025, ApJ, 986, 11
 Tamayo, D., Silburt, A., Valencia, D., et al. 2016, ApJ, 832, L22
 Tejada Arevalo, R., Tamayo, D., & Cranmer, M. 2022, ApJ, 932, L12
 Thadhani, E., Ba, Y., Rein, H., & Tamayo, D. 2025, Research Notes of the American Astronomical Society, 9, 27
 Weiss, L. M., Marcy, G. W., Petigura, E. A., et al. 2018, AJ, 155, 48
 Weiss, L. M., Millholland, S. C., Petigura, E. A., et al. 2023, 534, 863
 Wisdom, J. 1980, AJ, 85, 1122
 Wisdom, J. & Holman, M. 1991, AJ, 102, 1528

Appendix A: Stability of a system on the $\alpha = 1$ three-body resonance

Due to the fact that the systems in SPK1, SPK2, and SPK3 all start on the main diagonal (away from the 3BR $\alpha 1$), it is not possible to clearly identify the resonance patterns as a function of the initial longitudes in Fig. 14. We define a system with the same inner period ratio as $b382$, with the outer period ratio such that the system starts on top of the 3BR $\alpha 1$ (using Eq. 10), instead of having the same period ratio value for each pair. The result is shown in Figure A.1. The "long-lived" stripes correspond to the resonant angle $\phi = -2\lambda_2 + \lambda_3 = 0^\circ$. On the stripes, 2016, 612, and 6 systems survived for at least 10^4 , 10^5 , and 10^6 , respectively. These systems are initially outside a long-lived island (the one on top of the 14/13 and 13/12 2BRs) and are extremely tightly-packed, as the inverse initial inner period ratio represents $\sim 99\%$ of the Hill stability limit value.

Appendix B: More about the geometry of three-body resonances

In this section, we turn off gravitational interactions between planets such that the resonances become infinitely thin. We also consider only coplanar and circular orbits.

Let us introduce a time-dependent parameter,

$$\gamma(t) = \sum_{i=1}^{N_p-1} \cos [\lambda_{i+1}(t) - \lambda_i(t)], \quad (B.1)$$

where N_p is the number of planets in the system. This parameter γ represents the sum of the difference in angle between adjacent pairs of planets and, therefore, characterizes the successive conjunctions as a function of time. When $\gamma(t) = N_p - 1$, all planets are in perfect conjunction. When $\gamma(t) = 1 - N_p$, then all consecutive pairs of planets are in opposite phase.

In the case of a three-planet system, Eq. B.1 reads

$$\gamma(t) = \cos [\lambda_2(t) - \lambda_1(t)] + \cos [\lambda_3(t) - \lambda_2(t)]. \quad (B.2)$$

When $\gamma = 0$, then the sum of the difference in longitude between each consecutive planet is 180° , so when a conjunction of two successive planets occurs, the other planet is in opposite phase. The resonance 3BR $\alpha 1$ is the only resonance where γ can remain constantly equal to zero, in this case during a two-planet conjunction, the other planet is in opposite phase.

Considering $\lambda_i = n_i t + \lambda_{i,\text{init}}$ and noting $\omega_{ji} = n_j - n_i$, Eq. B.2 becomes

$$\gamma(t) = \cos [\omega_{21} t + \lambda_{2,\text{init}}] + \cos [\omega_{32} t + (\lambda_{3,\text{init}} - \lambda_{2,\text{init}})], \quad (B.3)$$

where $\lambda_{i,\text{init}}$ is the initial angle of the i th planet at the start of integration (note that $\lambda_{1,\text{init}} = 0$). This represents the sum of two periodic waves with different frequencies and phases. The sum of two cosine can be written as the product of two cosine such that

$$\gamma(t) = 2A \times B \quad (B.4)$$

where

$$A \equiv \cos \left[\left(\frac{\omega_{21} - \omega_{32}}{2} \right) t + \left(\frac{2\lambda_{2,\text{init}} - \lambda_{3,\text{init}}}{2} \right) \right], \quad (B.5)$$

and

$$B \equiv \cos \left[\left(\frac{\omega_{21} + \omega_{32}}{2} \right) t + \frac{\lambda_{3,\text{init}}}{2} \right]. \quad (B.6)$$

The time-dependent term in Eq. B.5 can be written as

$$\frac{\omega_{21} - \omega_{32}}{2} = -\frac{1}{2} [n_1 - 2n_2 + n_3]. \quad (B.7)$$

In the case where the system is captured in a 3BR, the term inside the brackets can be written as

$$n_1 - 2n_2 + n_3 = \frac{q-p}{p} (n_2 - n_3). \quad (B.8)$$

If the system is captured in the 3BR $\alpha 1$, the time-dependent term in Eq. B.5 is equal to zero. The parameter γ is therefore a periodic function with a constant amplitude A that depends only on the phase shifts of the outer two planets $2\lambda_{2,\text{init}} - \lambda_{3,\text{init}}$. The amplitude is $A = 0$ when the phase shifts is $\pm\pi$ (when $\phi = \pi$). The third planet is exactly in opposite phase during all successive two-planet conjunctions. On the other hand, if $\phi = 2\pi$, then the amplitude $A = 2$ and a perfect three-planet conjunction occurs. The successive configurations are repeated systematically p times during the resonant period P_{3br} . The 3BR $\alpha 1$ is the only three-body resonance of the network with constant amplitude. For this specific resonance, the trajectory of $\cos(\lambda_3 - \lambda_2)$ vs. $\cos(\lambda_2 - \lambda_1)$ is an ellipse in phase space, whose eccentricity depends on the longitude shift. If the resonant angle is $\phi = \pi/2$, then the trajectory is a circle of radius 1, whereas if $\phi = 2\pi$ or π , the trajectory is a positive or negative diagonal line, respectively.

All 3BRs with the same α value, i.e., all resonances such that $q/p = q_l/p_l$ where p_l and q_l are the lowest terms, will show the same periodic curve of γ ; however, the period P_{3br} increases by a factor N , where $N \in 1, 2, \dots$ is the greatest common factor for p and q . The number of times the pattern repeats during P_{3br} therefore increases by N . This means that the lowest terms define the geometry of the resonance since all resonances with the same α value have the same trajectory in phase space (only the period changes). If $q_l - p_l$ is an even number, then the behavior of γ during the second half of the period P_{3br} is the symmetry of the first half along the time axis:

$$\gamma(t > P_{3br}/2) = -\gamma(t < P_{3br}/2), \forall t \in [0, P_{3br}]. \quad (B.9)$$

This illustrates, similarly to second-order 2BRs, that the system goes back to the initial configuration in opposite phase (all initial angles are shifted by 180° in inertial space) after a period $P_{3br}/2N$.

Let us now turn on gravitational interaction between planets. Figure B.1 displays the trajectory of γ in phase space for the numerically integrated system $b382$. We compare two sets of initial longitudes: one that keeps the system stable (from the Specific Set S1) and another that leads to quick instability. The stable integrated system follows the pattern predicted for a system in the 3BR $\alpha 1$ (see the red curve) as it is effectively trapped by this resonance (Fig. 12). We can see that the value of γ is always well below 1, which means that the system always remains very far from a three-planet close approach. On the other hand, the value of γ in the unstable system does not follow the resonant pattern and exhibits multiple three-planet close approaches.

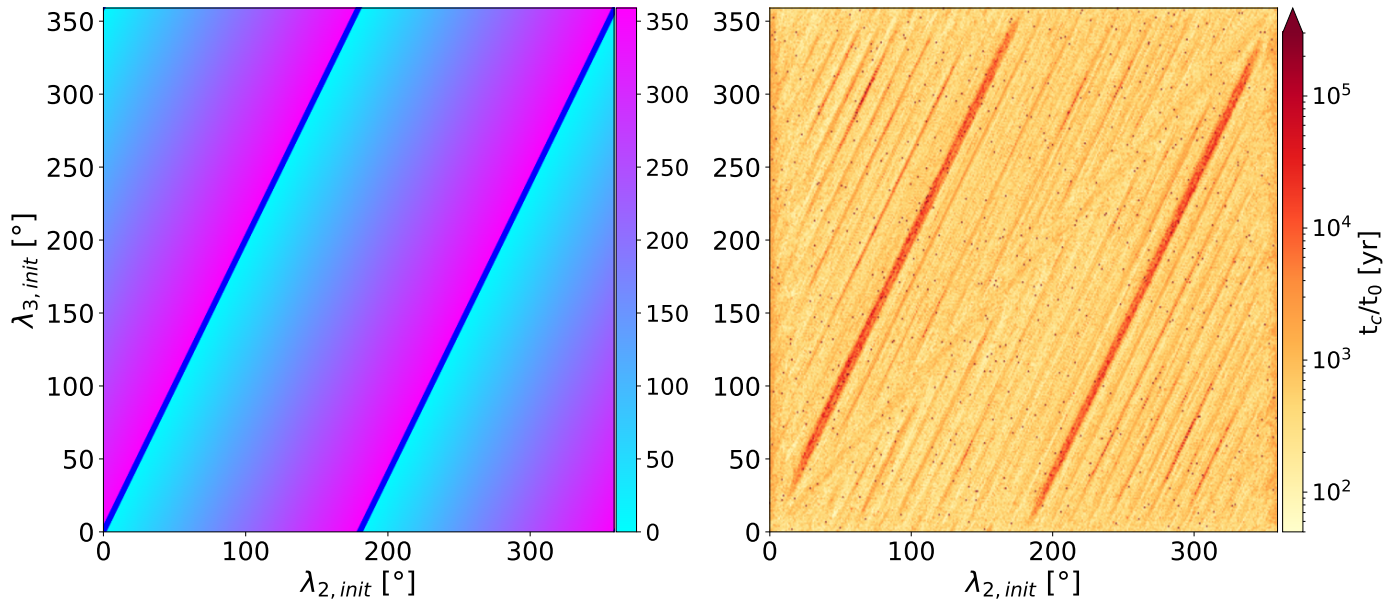


Fig. A.1: Left: resonant angle ϕ with $p = 1$ and $q = 1$ for all values of the angles λ_2 and λ_3 . The blue stripes correspond to $\phi = 0^\circ$. Right: Same as Fig. 7, but for the system $P_1/P_2 = 0.930$ and $P_2/P_3 = 0.925$ that starts on top of the 3BR.

The result shows that the trajectory of γ in the stable system is equivalent to that of a system with no planet-planet interaction; the net gravitational energy is perfectly balanced during the resonant period. We also examine the system *b541* with the initial longitudes (Sect. 6.1) and compare it to a different initial set of longitudes that leads to instability (Fig. B.2). Similarly, the stable system shows a pattern of γ that remains purely shaped by the 3BR $\alpha^{\frac{10}{9}}$.

Appendix C: Two-body resonance angles

Figures C.1, C.2, C.3 and C.4 show the early evolution of the two-body resonance angles in the direct vicinity of long-lived systems *b347*, *b382*, *b415*, and *b451*, respectively. Almost all angles circulate, and none of them clearly librates, even within a limited range in time. It is not possible to conclude that these systems are also locked in two-body mean motion resonance in addition to three-body resonance.

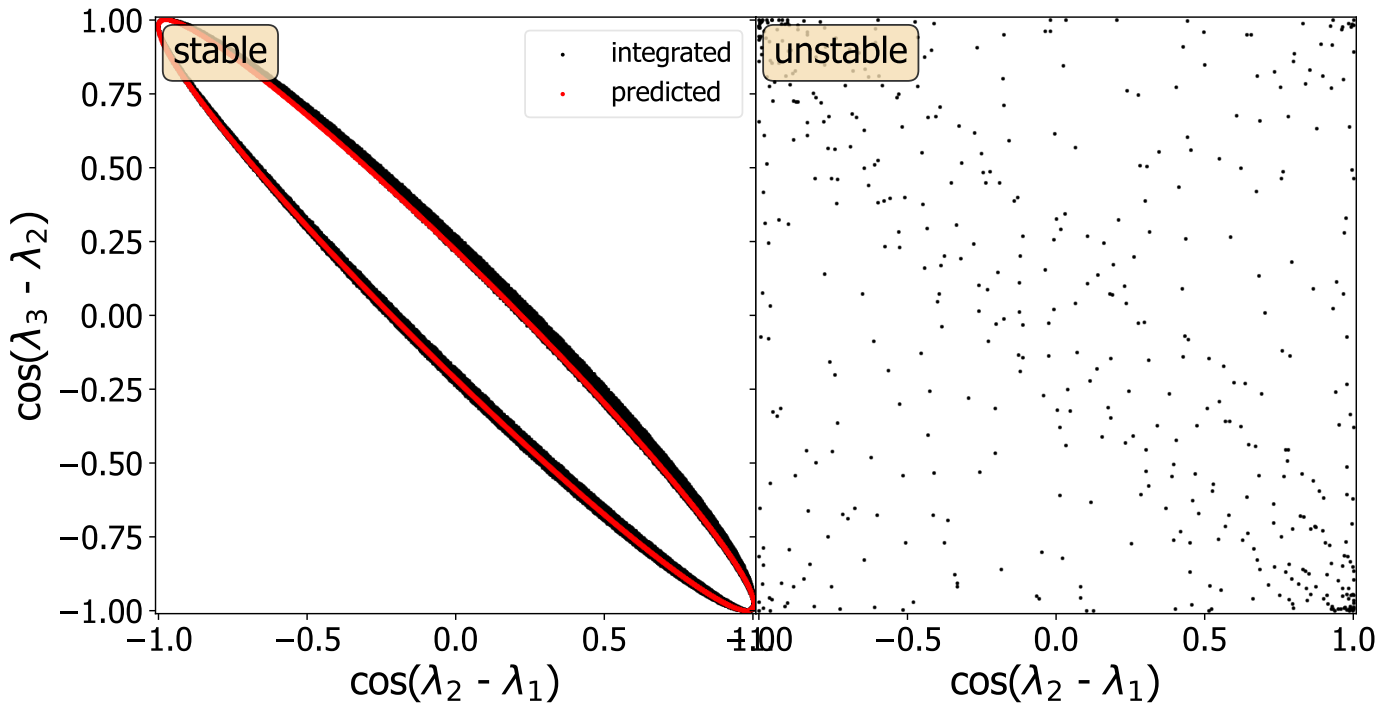


Fig. B.1: Phase space diagram of γ for two systems with the same initial $\beta = 3.82086$, but each with a different initial set of longitudes. The left panel shows γ for the stable system *b382* (Specific Set #1) and the right panel for a chosen set of initial angles ($\lambda_2 = 155^\circ$ and $\lambda_3 = 50^\circ$) that quickly leads to chaotic regime. In the right panel, the trajectory is shown for the first 500 years, which roughly corresponds to the unstable system's lifetime, while it is shown for 10^8 years of integration for the stable system. In the left panel, the red line is the predicted trajectory in phase space using Eq. B.3 (when the planet-planet gravitational interaction is turned off) with the same initial parameters as the stable integrated system.

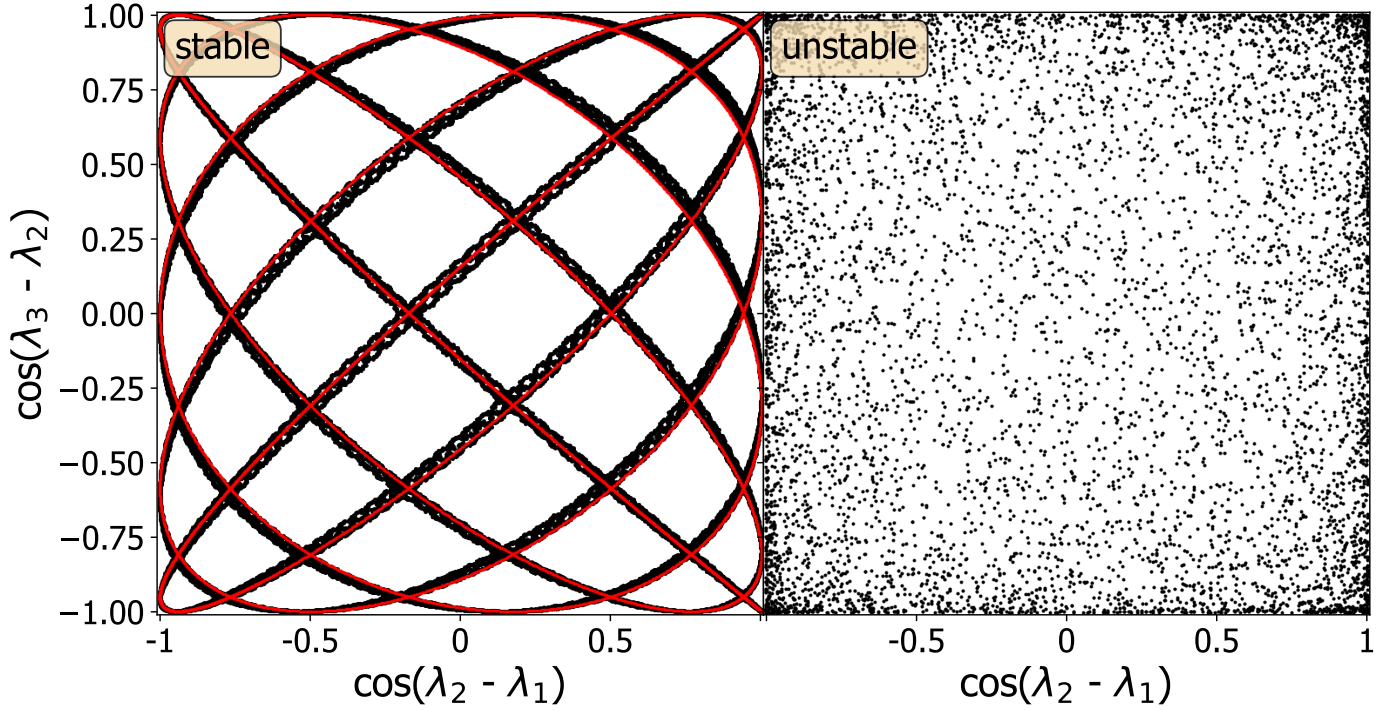


Fig. B.2: Phase space diagram showing the trajectory of γ of two systems with the same initial $\beta = 5.4135$, but each with a different initial set of longitudes. The left panel shows γ for the stable configuration $b541$ ($\lambda_2 = 228.2280^\circ$ and $\lambda_3 = 145.7270^\circ$) and the right panel an unstable configuration ($\lambda_2 = 230^\circ$ and $\lambda_3 = 65^\circ$). For the unstable systems, the initial angle values are chosen so they are away from the black stripes in Fig. 7. This system became unstable after about 24,000 years but the trajectory is shown during the first 500 years for visibility. The trajectory is shown for 10^8 years of integration for the stable system. The red line is the predicted trajectory using Eq. B.3 (when the planet-planet gravitational interaction is turned off) with the same initial parameters as the integrated system.

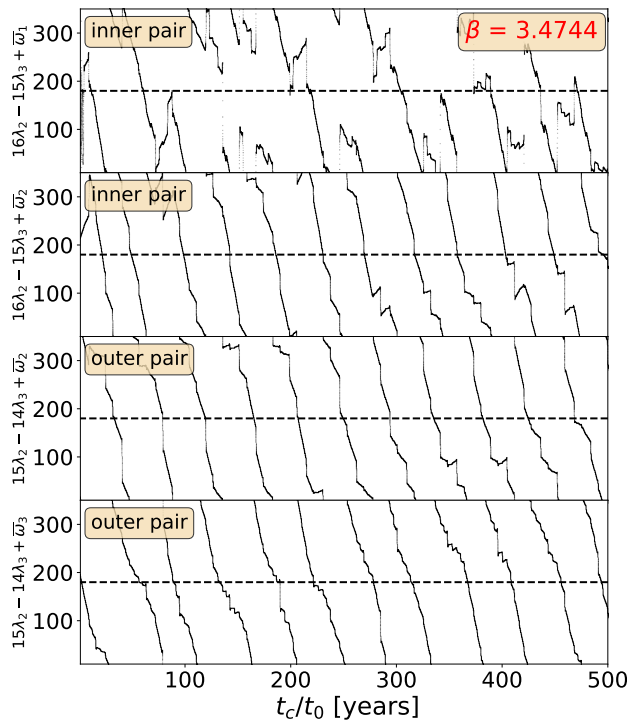


Fig. C.1: Evolution of the first-order two-body resonant angles, 14:15 and 15:16, over the first 1000 orbits of system $\beta = 3.4744$ in Set S2. Every angle circulates.

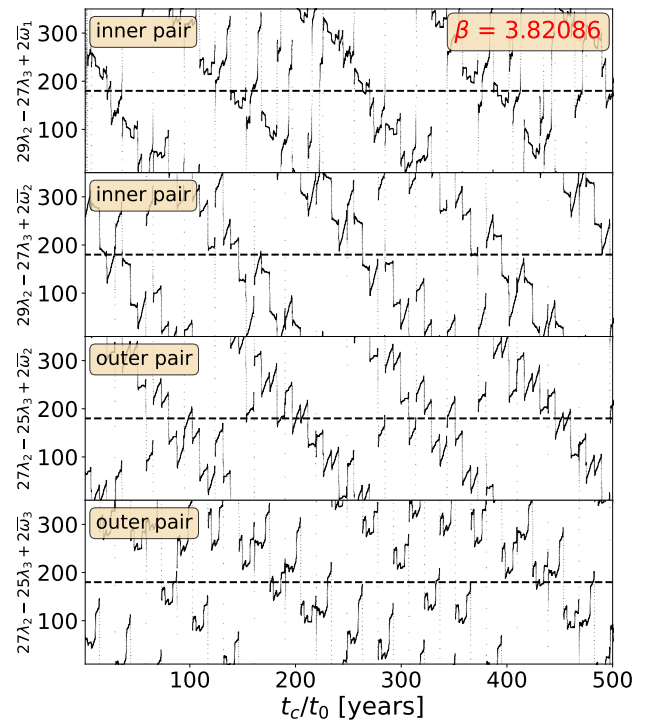


Fig. C.2: Evolution of the second-order two-body resonant angles, 25:27 and 27:29, over the first 1000 orbits of system $\beta = 3.82086$ in SPK1. Every angle circulates.

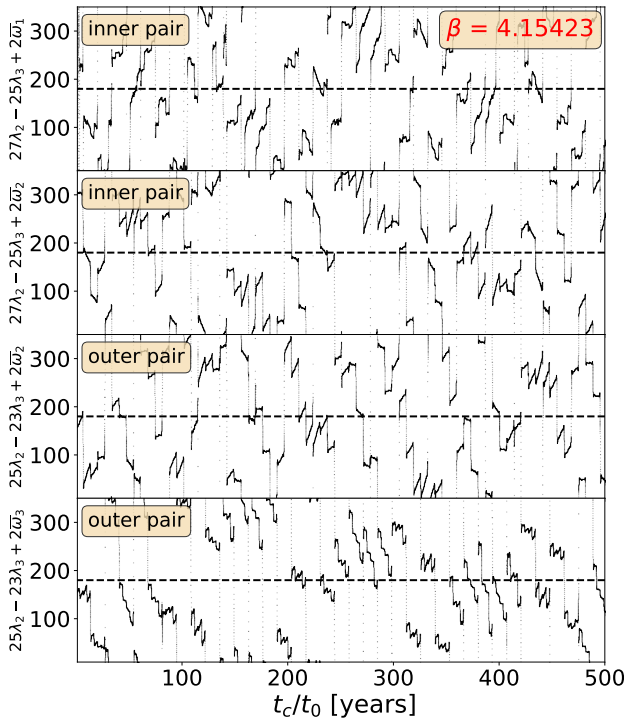


Fig. C.3: Evolution of the second-order two-body resonant angles, 23:25 and 25:27, over the first 1000 orbits of system $\beta = 4.15423$ in SPK2. The angles seem to circulate.

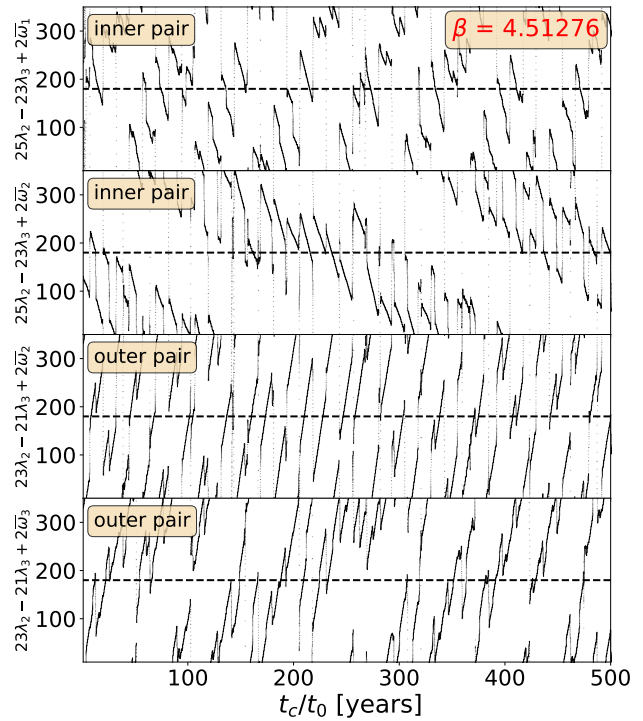


Fig. C.4: Evolution of the two-body resonant angles, 21:23 and 23:25, over the first 1000 orbits of system $\beta = 4.51276$ in SPK3. Every angle circulates.